Chapter 10
Closed Battery Systems

Akiko Tsurumaki, Sergio Brutti, Giorgia Greco, and Maria Assunta Navarra

Contents

10.1 Lithium Metal Batteries

Electrochemical plating/stripping of lithium metal at the negative electrode of aprotic batteries can in principle provide significant functional improvements compared to Li ion intercalation electrodes, in terms of the outstanding performance of the Li metal electrode (theoretical capacity = 3860 mAh g^{-1} and $E° = -3.04$ V vs. SHE, standard hydrogen electrode, cf. 372 mAh g^{-1} and ≈ -2.9 V vs. SHE for graphite) [1]. A high energy density of 400–600 Wh kg^{-1} can be achieved when lithium metal anode is combined with intercalation-type cathode materials such as $LiFePO_4$, $LiCoO_2$, lithium–nickel–manganese–cobalt oxide (NMC), and lithium–nickel–cobalt–aluminum oxide (NCA). The use of Li metal anode is also proposed in Li–sulfur (Li–S) batteries and Li–oxygen ($Li–O_2$) batteries, thus enabling further increase in the energy density of these

A. Tsurumaki · S. Brutti · G. Greco · M. A. Navarra (✉)
Department of Chemistry, Sapienza University of Rome, Rome, Italy
e-mail: akiko.tsurumaki@uniroma1.it; sergio.brutti@uniroma1.it; giorgia.greco@uniroma1.it; mariassunta.navarra@uniroma1.it

S. Passerini et al. (eds.), *Emerging Battery Technologies to Boost the Clean Energy Transition*, The Materials Research Society Series,
https://doi.org/10.1007/978-3-031-48359-2_10

next-generation battery chemistries. However, and despite the extraordinary research efforts made in the last five decades by researchers all over the word, lithium metal electrodes in secondary, i.e., rechargeable, batteries are still far from being commercially feasible. In fact, there are fundamental limitations that hinder the reversibility of lithium metal stripping/deposition in aprotic electrolytes based on liquid, polymer, or crystalline components [2].

In the lithium metal battery (LMB) technology, the reduction potential of Li is below that of conventional organic electrolytes. Therefore, lithium metal electrodes show Coulombic efficiencies upon cycling lower from unity in batteries. This fact makes the electrolyte a critical component in the development of LMB. In addition, the uneven deposition morphology of Li and inhomogeneous electrochemical dissolution lead to dendrite and dead lithium formation, lowering the Coulombic efficiencies [3]. A wide variety of approaches has been proposed to tackle these drawbacks, rooted in thermodynamics and kinetics of the lithium stripping/deposition. Overall, the electrochemical reversibility of lithium metal electrodes can be enhanced by the following four main strategies [4]:

1. Optimization of the electrolyte formulation to control the solid electrolyte interphase (SEI) formation over the electrodes
2. Pre-deposition of an artificial SEI over the lithium metal electrode
3. Exploitation of open three-dimensional scaffolds with controlled meso- or nanomorphologies to buffer volume expansions and self-heal the formation of dead lithium
4. Substitution of liquid electrolytes with solid polymer and inorganic materials, and their combination into hybrid electrolytes, to limit side reactions at the lithium metal surface

10.1.1 Mechanism of the Electrochemical Lithium Stripping/Deposition in Liquid Electrolytes

Lithium metal is an extraordinary reducing agent with the redox potential of $E^{\circ} = -3.04$ V vs. SHE. Almost all aprotic liquid solvents with polar groups suitable for the formulation of secondary battery electrolytes are thermodynamically unstable in contact with lithium. This thermodynamic constraint causes an immediate degradation of solvent molecules in contact with the surface of lithium metal through a pseudo-corrosion mechanism [5]. The degradation is initiated by the irreversible reduction of one solvent molecule:

$$\mathrm{solvent} + \mathrm{Li} \rightarrow \mathrm{solvent}^{\bullet -} + \mathrm{Li}^{+}\,(\mathrm{solv})$$

and this reaction unavoidably creates pitting holes over the lithium metal through the release of solvated Li^+ ions in the electrolyte, simultaneously generating the unstable radical $\mathrm{solvent}^{\bullet -}$ anion in a doublet state [6]. This radical molecule easily undergoes further reactions with other solvent molecules:

$$\text{solvent}^{\bullet -} + \text{solvent} \rightarrow (\text{solvent–solvent})^{\bullet -}$$

to form a short-chain radical polymer $(\text{solvent–solvent})^{\bullet -}$. The radical can also react with the salt anion (e.g., $LiPF_6$) to form insoluble lithium salts like lithium fluoride:

$$\text{solvent}^{\bullet -} + \text{LiPF}_6\ (\text{solv}) \rightarrow \text{LiF}\ (\text{solid}) + (\text{PF}_5\text{–solvent})^{\bullet -}.$$

In turn, unstable alkyl carbonate–fluorophosphate adducts, i.e., $(PF_5\text{–solvent})^{\bullet -}$, are formed that easily further degrade through irreversible multistep processes, leading to a precipitation of the insoluble species and/or an alteration of the electrolyte composition. Another degradation process of the $\text{solvent}^{\bullet -}$ radical anion is its intramolecular breakup promoted by a further reduction, leading to the formation of gaseous species (i.e., molecular hydrogen, ethylene, and other small volatile organic molecules like formaldehyde, acetylene, etc.) [7]. These multifarious radical chain reactions, initiated by the inevitable reduction of solvent molecules, lead very rapidly to the precipitation of insoluble inorganic and organic by-products (e.g., Li_2CO_3, Li_2O, lithium alkyl carbonates, esters, etc.) over the surface the lithium metal, thus forming a passivation film (i.e., a natural solid electrolyte interphase, namely, n-SEI) [8]. This n-SEI completely passivates the surface of lithium metal, within the pitting holes as well as in the outer areas, but the pseudo-corrosion is not remarkable in the latter. Therefore, the n-SEI is unavoidably inhomogeneous in the nanometer scale, with significant compositional and morphological differences. Furthermore, in the initial electrochemical lithium deposition or oxidation of the lithium electrode, further electrolyte degradation occurs ending in the complete passivation of the surface by a thick passivation n-SEI film that is reminiscent of the original natural SEI [9].

The compositional inhomogeneity of the n-SEI originates from the so-called weak points, where the accumulation of organic by-products makes the local electric resistance larger compared to the surrounding areas of the electrode. These weak points become the most favorable nucleation sites for the electrochemical deposition of lithium metal and the electrochemical stripping of lithium ions. Overall, the surface of the lithium metal electrodes upon cycling will alter, driven by the local fluctuation of the n-SEI transport properties, thus leading to the aggravation of the original morphological inhomogeneities with formation of dendrites and pitting holes [10].

Once formed, dendrites increase remarkably the volume of the lithium metal electrode and grow preferentially toward the counter-electrode, following the electric field lines. This growth leads to internal short circuits and catastrophic cell failures. Moreover, dendrite formation exposes additional fresh lithium surface to the electrolyte, thus leading to further electrolyte degradation and accumulation of n-SEI. This mechanism is particularly unfavorable as it drives the formation of dead lithium upon stripping. This is because dendrites can be electrochemically dissolved during discharge, and therefore it is possible that a portion of the metallic lithium dendrite, passivated by the unfavorable n-SEI, may lose an electronic contact with

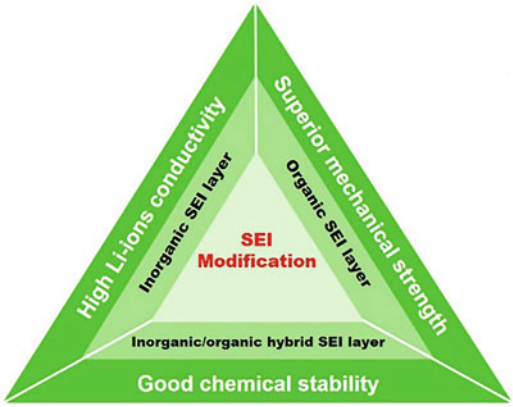

Fig. 10.1 Optimal properties of SEI layers over metallic lithium [12]

the bulk of the electrode. Unavoidably, these isolated lithium dendrites cannot undergo further electrochemical reactions leading to the loss of active material [11].

In general, the n-SEI grown on lithium metal before and upon cycling should meet several requirements to mitigate the dendrite growth, enhance the reversibility of plating/stripping, and suppress the formation of dead lithium as schematically summarized in Fig. 10.1.

Unfortunately, the n-SEI layer formed in typical LIB electrolytes is unable to fulfill these demands, and, as already mentioned, different strategies have been considered to tackle this challenge, in particular forming artificial SEI layers or altering the nature of the n-SEI. Another radical approach is to replace liquid electrolytes moving to solid-state (electrolyte) batteries.

10.1.2 SEI Modulation via In Situ Formation

The formation of the SEI can be modulated by electrolyte additives that can alter the degradation mechanism to form more homogeneous and stable passivation films over the surface of the lithium metal electrodes. These sacrificial chemical species initially consume some metallic lithium of the electrode, but this consumption is generally limited and will end once the lithium electrode surface is passivated in situ by a modified solid electrolyte interphase (m-SEI). These electrolyte additives belong to two main groups depending on their main effect, i.e., reduction-type and reaction-type additives [13].

Reduction-type additives have a relatively high redox potential and are reduced upon lithium deposition prior to any unfavorable effect on the electrolyte [14]. Their decomposition products form an insoluble film, protecting the electrode/electrolyte interface, with enhanced transport properties compared to the n-SEI formed spontaneously without the additive. Reduction-type additives are divided into two subgroups. The first subgroup consists of reactive compounds containing unsaturated

bonds like vinylene carbonate (VC) or fluoroethylene carbonate (FEC) and promotes the accumulation of polymerized organic species over the surface of the lithium metal electrodes. The second subgroup includes reductive agents aiding the SEI formation. This class of reductive additives is electrochemically reduced before the electrolyte decomposition by-products precipitate onto the lithium surface. These additives can also react with radical species generated during the initial solvent reduction process, thus terminating the radical chain reaction that leads to the uncontrolled n-SEI formation. The most common chemical species that belong to this class are sulfur-containing chemical like sulfolane, ethylene sulfite, or dialkyl-sulfone [15]. Their degradation ends with the formation of insoluble lithium sulfites or alkyl lithium sulfites.

Reaction-type additives are typically molecules with scavenging abilities. These species can react with intermediates of the natural degradation radical chain reaction of the electrolyte in contact with lithium surfaces, altering the final composition of the SEI by promoting the accumulation of electrochemically inert species with favorable transport properties. (Trimethylsilyl)isothiocyanate can easily scavenge PF_5 as well as phosphite-containing compounds, thanks to their strong nucleophilic character [16].

Besides reaction-type and reduction-type additives, it is important to mention the possible use of co-salts of multivalent cations (e.g., Mg^{2+}, Ca^{2+}, Zn^{2+} Fe^{2+}, In^{3+}, and Ga^{3+}). Many of these cations can alloy with lithium upon reduction worsening the ionic transport properties across the entire electrode surface. This effect leads to a smaller ionic conductivity but mitigates the uncontrolled growth of lithium dendrites [17].

10.1.3 Ex Situ Deposition of Artificial SEI

The second general strategy to improve the reversibility of lithium stripping/deposition is the ex situ preformation of an artificial SEI layer (a-SEI) on the surface of the metallic electrode. This strategy cannot fully prevent the spontaneous reactivity of the electrolyte with the lithium surface but can strongly mitigate its occurrence and therefore strongly reduce the chemical and morphological inhomogeneity of the lithium electrode surface. In general, a-SEIs over lithium metal electrodes can be synthesized by atomic-layer deposition (ALD), aeration, or chemical coating in a liquid precursor solution [18].

ALD is an advanced thin-film fabrication technique capable of producing homogeneous and ultrathin films at room temperatures or slightly above [19]. The final surface film is extremely thin, thanks to the careful control of the mass-loading of the a-SEI allowed by the technique. These ultrathin films are typically constituted by Al_2O_3 that, during the electrochemical deposition of lithium, firstly converts into the highly conductive lithium aluminate $Li_xAl_2O_3$ that stabilizes further the a-SEI and allows a remarkable limitation of the dendrite growth [20].

Aeration is a chemical deposition method from the gas phase, in which the lithium metal surface reacts with almost permanent gaseous species like N_2 or O_2 to form homogeneous nitride or oxide layers. Since Li_3N is an electrochemically stable and fast ion conductive chemical species, the precipitation of a continuous and homogeneous thin film of lithium nitride over the surface of lithium metal acts to prevent side reactions between lithium metal and the electrolyte without hindering the lithium ion mobility [21].

The a-SEI, starting from selected liquid precursor solutions, can be obtained by using the so-called dip-coating or drop-casting method. A suitable chemical composition of the precursor solutions promotes the formation of a-SEI with controlled compositions and surface moieties. In fact, the constituent species of the precursor solution degrades due to the direct chemical reaction with the metallic lithium forming a preliminary passivation film [22]. This a-SEI can mitigate the unavoidable reactivity of the metallic lithium surface with the electrolyte upon cycling. The composition of the precursor solutions can modulate the composition of the resulting a-SEI allowing the control of the transport and mechanical properties of the a-SEI. An almost innumerable number of precursor solutions have been proposed in the literature, all leading to an improvement in the overall reversibility of the lithium plating/stripping. Among the many possibilities, one that should be mentioned is the use of polyphosphoric acid solution in organic solvents like dimethyl sulfoxide that promotes the formation of a Li_3PO_4-rich a-SEI, with excellent chemical stability, high Young's modulus (10–11 GPa), and high lithium ion conductivity [23].

10.1.4 3D Engineering of the Electrode Morphology

The third possible approach is to modify the morphology of the surface where Li is plated (either Li metal or directly the current collector) by an engineering at the nanoscale. Mechanically robust and chemically inert three-dimensional scaffolds or generic frameworks are used to facilitate homogeneous deposition of lithium metal, thus indirectly limiting the degradation of the electrolyte over fresh lithium surface [24]. The coating of lithium metal electrodes with very thin amorphous carbon-based hollow nanostructures can modulate the Li^+ ion transport pathways toward the metal surface, leading to the nucleation and growth of the lithium deposits either over Li or the current collector. Furthermore, lithium metal can deposit within the hollow nanostructures with a minimal contact with the electrolyte, thus mitigating any further degradation. Also, the use of two-dimensional materials like graphene or hexagonal boron layer can modulate the lithium stripping/deposition reaction by inducing specific growth morphologies and the formation of a tailored a-SEI [25].

The use of open nickel foams as a current collector and support for the lithium deposition is also an effective strategy to accommodate the huge volumetric changes experienced by conventional host-less flat electrodes to lead homogeneous lithium deposition. In fact, the 3D open foam can be infused with molten lithium by capillary force forming a composite scaffold with a minimized interfacial resistance and empty spaces to buffer volumetric changes upon stripping and deposition [26].

10.2 All-Solid-State Lithium Metal Batteries

The use of commercially available organic liquid electrolytes in LMBs, as well as in Li ion batteries (LIBs), unavoidably poses major safety issues because of their flammability and strongly exothermic reactivity with lithium that can easily self-heat the battery in case of accidents, leading to catastrophic explosions. The replacement of liquid electrolytes with a solid electrolyte (SE) allows to tackle this serious drawback drastically and reduces the risk of fire and explosion even in case of major thermal, mechanical, or electrical abuse. As a further advantage, the use of SEs as an electrolyte having a function of separator increases the overall volumetric energy density of the batteries, thus improving the overall performance [27].

The ideal set of properties of SEs is [28, 29]:

1. High ionic conductivity ($>10^{-4}$ S cm^{-1}, better $>10^{-3}$ S cm^{-1} in the case of thick composite electrolytes) with a high Li^+ transference number (t_{Li+}), especially at low temperatures
2. Good chemical compatibility with other battery components including lithium metal
3. Good thermal and electrochemical stability at a wide range of temperatures and voltages for the constant operation of cells, including the thermal stability also in terms of the absence of phase transition so as to avoid the formation of low conductive solid phase
4. Minimal interfacial resistance between SE and electrodes
5. High electronic area-specific resistance, resulting in conductivities $<10^{-12}$ S cm^{-1}, to prevent self-discharge
6. Appropriate mechanical strength to resist dendrite growth
7. Good affordability in terms of less environmental impact, allowing for simple and low cost fabrication of both SE itself and devices

All-solid-state batteries with lithium metal electrodes (ASS-LMB) are classified as "generation 4b batteries" by the EU commission. However, despite the excellent functionality of SEs, several drawbacks hinder their development beyond the lab-scale and the final commercialization. The most relevant challenges are the unsatisfactory ionic conductivity compared to classical liquid electrolytes, the large impedance at the electrode–electrolyte interfaces, and the electrochemical instability against lithium metal of SE constituents.

10.2.1 Classification of Solid Electrolytes

Solid-state electrolytes can be either inorganic solid electrolytes (ISEs), solid polymer electrolytes (SPEs), or their composites. The former electrolyte can further be divided into oxide types, sulfide types, and others including hydride, borate, and

phosphate types. The oxide-type ISEs have good chemical and electrochemical stability. The design of a material with a good air stability and low toxicity is possible. They exhibit a fast ionic conductivity in bulk, up to 10^{-3} S cm^{-1} at room temperature; however, to achieve this ionic conductivity, a sintering procedure at high temperatures, conventionally at around 1000 °C, is necessary to reduce grain boundary resistance between electrolyte particles. In contrast to this, sulfide-type ISEs have a low oxidation stability and high reactivity in the presence of moisture but exhibit a high ionic conductivity merely by pressing the materials at room temperature (so-called low-temperature sintering). This is because of a larger size S^{2-} which broadens ion conduction pathways in the electrolyte structure and the higher polarizability of S^{2-} which weakens the interaction with Li^+. On the other hand, SPEs have several advantages in manufacturing processes, such as simple production of large-area films, easy formation of a seamless interface with the electrodes, and possible handling of SPE in ambient air. However, it is not easy to find a suitable combination of a polymer matrix and additive salt that can exhibit ionic conductivity higher than that of ISEs, except for the combinations forming gel polymer electrolytes.

10.2.2 Ion Conduction Mechanisms of Solid Electrolytes

ISEs normally consist of two sublattices: a crystalline framework composed of immobile ions and a sublattice of mobile ions [30]. Therefore, Li^+ ions move within an essentially static framework through ion hopping (i.e., the Grotthuss mechanism), which is favorable with regard to a faster ion conduction. The mobile species in a crystalline solid need to pass through periodic bottleneck points, which defines migration energy. To reduce the energy barrier and achieve faster ion conduction, (1) the number of mobile ions and their hopping sites, as well as the vacancy of the mobile ions, (2) the size of bottleneck points, (3) the degree of structural order in a mobile ion sublattice, and (4) the presence of highly polarizable anions in sublattices are critical factors [31]. In glassy inorganic materials, the ion conduction mechanisms are quite like those in crystalline structures. The ions at local sites, being excited to neighboring sites, diffuse collectively on a macroscopic scale. In contrast to these, in SPEs, the motion of Li^+ ions is mediated by the dynamics of the host polymer, i.e., the vehicular mechanism, thereby restricting the ion conduction to a relatively slow speed. The segmental motions of polymer chains create free volumes that allow for the migration of ions coordinated by the polymer polar groups, and ions migrate from one coordinate site to another, promoted by the segmental motions. The ionic conductivity, in this case, is strongly dependent on the crystallinity of the host polymer.

10.2.3 Development of Inorganic Solid Electrolytes

The diffusion of ions in crystalline solids is significantly affected by both ion valence and ionic radius of the migrating species because these influence electrostatic interactions between mobile ions and cations forming the structural skeleton [31]. In addition to this, the natures of the ligands and metals composing the skeleton of the host framework have large impacts on the performance of ISEs because they determine the channel size for ion migration. In the case of Li^+ diffusion, since controlling the bottleneck size for the ion diffusion has been successful in enhancing Li^+ conductivity and reducing the activation energy, structural tuning by cation substitutions within a given structural framework has been intensively studied. Among those investigated, the most attractive Li^+ conductors, based on oxides such as natrium super ionic conductor (NASICON) type, garnet type, and perovskite type, as well as sulfides such as lithium super ionic conductor based on sulfides (thio-LISICON) type, $Li_{10}MP_2S_{12}$ (LGPS) type, argyrodite type, and $Li_7P_3S_{11}$ type, are summarized in this section and Table 10.1.

NASICON-Type (e.g., LATP/LAGP) NASICON-type Li^+ conductors are represented by the general formula of $AM_2(PO_4)_3$, in which A = Li and M = Ge, Ti, Zr, etc., forming a three-dimensional framework of MO_6 octahedra alternatively connected with PO_4 tetrahedra by sharing their vertices [31]. Lithium ions occupy two different sites in the structure, so-called A1 and A2 sites, and their migration occurs via ion hopping between these sites. The limitation for the ion motion comes from triangular oxygen windows, which separate the A1 and A2 sites, known as the bottleneck [38]. Therefore, optimization of the bottleneck size effectively improves the ionic conductivity and reduces its activation energy.

The first strategy for this issue is the use of larger M ion in $AM_2(PO_4)$ structure [33]. For example, the ionic conductivity of $LiGe_2(PO_4)_3$ is only 6.62×10^{-9} S cm^{-1} [32]. In the case of $LiTi_2(PO_4)_3$ and $LiZr_2(PO_4)_3$, where Ge^{4+} is replaced with larger ions, their ionic conductivities improve to 2×10^{-6} S cm^{-1} and 3.8×10^{-5} S cm^{-1} at room temperature, respectively. The second strategy is the aliovalent substitution, resulting in $A_{1+x}M'_xM_{2-x}(PO_4)_3$, in which M′ = Al, Ga, La, etc. This increases the Li^+ concentration and also its mobility [33]. The concentration of M^{3+} needs to be limited to ~15% (x = 0.3) to avoid the formation of a secondary phase due to an ionic radius mismatch [31]. Al-doped NASICON-type materials, such as $Li_{1+x}Al_xTi_{2-x}(PO_4)_3$ (LATP) and $Li_{1+x}Al_xGe_{2-x}(PO_4)$ (LAGP), are known to exhibit ionic conductivities of ~3×10^{-3} S cm^{-1} (when x = 0.3) [31] and 1.0×10^{-3} S cm^{-1} (when x = 0.5), respectively [33]. Both LATP and LAGP are stable at relatively high potentials and in air, while they are unstable at low potentials because Ti^{4+} is easily reduced. The formation of a protective layer based on polymers, LiPON, or other ISEs allows the use of this kind of materials with lithium metal anodes [39].

Garnet-Type (e.g., LLZO) The general formula of garnet-type materials is $A_3B_2(XO_4)_3$, in which A = Ca, Mg, Y, La, etc., B = Al, Fe, Ga, Ge, Mn, Ni, V, etc., and X = Si, Ge, Al, etc., forming eightfold, sixfold, and fourfold coordinated

Table 10.1 Properties of different kinds of ISEs

Structure type	Basic structure	Particular composition	Conductivity at R.T./ S cm^{-1}	Advantage/ disadvantage	[Ref]
Oxides					
NASICON	$AM_2(PO_4)_3$ A site for Li^+	$LiTi_2(PO_4)_3$	2×10^{-6}	High air stability/incompatible with lithium metal anode because of Ti^{4+} with poor resistance to reduction	[32]
		$Li_{1+x}Al_xTi_{2-x}(PO_4)_3$ (LATP)	$\sim 3 \times 10^{-3}$ (x = 0.3)		[31]
		$Li_{1+x}Al_xGe_{2-x}(PO_4)_3$ (LAGP)	1.0×10^{-3} (x = 0.5)		[33]
Garnet	$A_3B_2(XO_4)_3$ X site for Li^+	$Li_7La_3Zr_2O_{12}$ (LLZO)	1.63×10^{-6} (tetragonal)	Stable against lithium metal/ lithiophobic	[34]
		$Li_7La_3Zr_2O_{12}$ (LLZO)	2.44×10^{-4} (cubic)		[32]
		$Li_{6.24}Al_{0.24}La_3Zr_2O_{11.98}$	4×10^{-4}		[35]
		$Li_{6.4}Ga_{0.2}La_3Zr_2O_{12}$	1.32×10^{-3}		[35]
Perovskite	ABO_3 A site for Li^+	$Li_{3x}La_{2/3-x}\square_{1/3-2x}TiO_3$ ($0 < x < 0.167$, LLTO)	$\sim 10^{-3}$	Presence of grain boundary resistance, incompatible with lithium metal anode because of Ti^{4+}	[32]
Sulfides					
Thio-LISICON	$Li_xM_{1-y}M'_yS_4$	$Li_{3.25}Ge_{0.25}P_{0.75}S_4$	2.2×10^{-3}	High ionic conductivity (merely after pressing)/limited stabilities in the contact with moisture and lithium	[36]
LGPS	$Li_{10}MP_2S_{12}$	$Li_{9.54}Si_{1.74}P_{1.44}S_{11.7}Cl_{0.3}$	2.5×10^{-2}		[32]
Argyrodite	Li_6PS_5X	Li_6PS_5Cl	1.9×10^{-3}		[36]
		Li_6PS_5Br	6.8×10^{-3}		
$Li_7P_3S_{11}$	Li_2S–MS_n	$Li_7P_3S_{11}$	1.7×10^{-2}		[37]

structures centered on A, B, and X cations, respectively [32]. Li^+-conductive garnets have the general composition of $A_3B_2(LiO_4)_3$. The Li^+ content can be increased by the aliovalent doping, and several materials with different stoichiometry such as the Li3 series, $Li_3Ln_3Te_2O_{12}$ (Ln = Y, Pr, Nd, etc.), Li5 series, $Li_5La_3M_3O_{12}$ (M = Nb, Ta, Sn, etc.), Li6 series, $Li_6ALa_2M_2O_{12}$ (A = Ca, Sr, Ba, etc., and M = Nb, Ta, etc.), and L7 series, $Li_7La_3M_2O_{12}$ (M = Zr, Sn, Hf, etc.), have been reported [32]. Garnets with Li^+ concentration > 3, e.g., $Li_7La_3Zr_2O_{12}$ (LLZO), are identified as stuffed lithium garnets [40]. In these stuffed lithium garnets (i.e., Li5-7 series), Li^+ occupies both tetrahedral and highly distorted octahedral coordination sites, while in the conventional garnets (i.e., Li3 series), Li^+ occupies only a tetrahedral coordination. Li ions in octahedral site migrate easily, while those in the tetrahedral site are not.

In the case of Li7 series garnet-type materials, including LLZO, the material can possess a cubic phase featuring a disordered lithium arrangement in addition to a tetragonal phase featuring a fully ordered lithium occupancy [32, 35]. The formation of a cubic structure is critical to achieve a high level of ionic conductivity. Aluminum doping is known to stabilize the cubic phase of LLZO and enhance Li^+ conductivity in one to two orders of magnitude compared to undoped tetragonal LLZO [35]. Furthermore, the ionic conductivity can be increased to 1.32×10^{-3} S cm^{-1} by doping Ga^{3+} [35]. Regarding the electrochemical stability, garnet-type electrolytes are favorable in terms of showing a stability against lithium metal. In the case of LLZO, however, the material is lithiophobic [41], resulting in a formation of the interphase with a high charge transfer resistance. Softening of the lithium at 170–175 °C (about 5–10 °C below Li melting temperature) [1] and the formation of lithiophilic coating such as those based on ionic liquids or polymers [42, 43] are known to be an effective solution for this problem. Instability at the interface with cathode has also been reported. The coating formation is effective also in this case in preventing oxidations of the electrolyte.

Perovskite-Type (e.g., LLTO) Perovskite structures are described as follows: ABO_3, in which the A-site ions (typically divalent alkaline earth metal ions) locate at the corners of a cube structure, B ion (typically transition metal ions, such as Ti^{4+}) at the center, and oxygen atoms at the face-centered positions. Based on this framework, 12-fold coordination is formed around A sites and sixfold coordination (BO_6) around B sites by a sharing corner with each other [31]. A Li^+ conductor can be obtained by replacing the divalent alkaline earth metal ions at A sites with the trivalent rare-earth element such as La^{3+} and monovalent Li^+. Just like the other ISEs, the bottleneck size for the ion conduction needs to be controlled to improve ionic conductivity, and this has been done by introducing large rare-earth or alkaline earth metal ions in the A site [31]. The presence of vacancy in the material, more specifically $Li_{3x}La_{2/3-x}\square_{1/3-2x}TiO_3$ (LLTO, $0 < x < 0.167$, $\square$ represents vacancy), for example, also allows for the enhanced bulk conductivity of $\sim 10^{-3}$ S cm^{-1} at room temperature. In such materials, La-rich and La-poor (i.e., Li-rich) layers are formed and alternately stacked. Within this structure, Li^+ transport is restricted to the Li-rich layers, and minimal transport occurs between these layers, which limits Li^+ transport to be two-dimensional. In polycrystalline structures, Li-rich layers in each grain are misaligned, and this reduces the ionic conductivity of the materials one to two orders of magnitude lower than that of the bulk [44]. As observed in other materials containing Ti^{4+} with less resistance to reduction, LLTO is not stable in a low-potential region, making it incompatible with the lithium metal anodes. Therefore, the partial or complete substitution of Ti^{4+} with Sn^{4+}, Zr^{4+}, Mn^{4+}, and Ge^{4+} has been reported. These modifications need to be carried out so as not to form a secondary phase and not to decrease the Li^+ concentration in the materials [45].

Thio-LISICON-Type and LGPS-Type Thio-LISICON-type electrolytes can be obtained by substituting O^{2-} by S^{2-} in a LISICON structure, specifically from $Li_xM_{1-y}M'_yO_4$ to form $Li_xM_{1-y}M'_yS_4$ (M = Si or Ge; M′ = P, Al, Zn, Ga, etc.) [29]. The thio-LISICON-type electrolytes exhibit higher ionic conductivity

compared with the LISICON electrolytes [31]. This is because of a larger size and higher polarizability of sulfide ions as discussed before for the classification of SEs. Depending on the valence of the cations, lithium vacancies in the structure can be controlled which affect Li^+ conduction significantly [46]. The maximum conductivity of the thio-LISICON family can be as high as 2.2×10^{-3} S cm^{-1} in the case of $Li_{3.25}Ge_{0.25}P_{0.75}S_4$ [36]. Thio-LISICON-type electrolytes tend to be unstable faced with lithium metal. However, their high ionic conductivity established this class of electrolytes as potential ISEs for the future of ASS batteries.

$Li_{10}MP_2S_{12}$ (M = Si, Ge, or Sn) and $Li_{11}Si_2PS_{12}$ are frequently considered as one of the thio-LISICON-type electrolytes [31]. However, thio-LISICON-type and these electrolytes have different crystalline structure, specifically based on orthorhombic and tetragonal crystal systems, respectively [47], and therefore can be regarded as different class of materials, namely, LGPS type. The electrolyte consists of $(Ge/P)S_4$ tetrahedra alternating with LiS_6 octahedra, forming a one-dimensional chain along the c-axis by sharing a common edge. These linear chains are connected to each other by PS_4 tetrahedra by sharing a vertex with LiS_6 octahedra [36], forming a backbone structure. Lithium ions locate in the empty space of the backbone structure by forming LiS_4 tetrahedra and create a one-dimensional LiS_4 chain along the c-axis, which is available for Li^+ conduction. In addition to this conductive channel, Li^+ diffusion is possible between neighboring conduction paths through the LiS_6 tetrahedra. Aliovalent doping enhances ionic conductivity, and, in particular, $Li_{9.54}Si_{1.74}P_{1.44}S_{11.7}Cl_{0.3}$ exhibits ionic conductivity of 2.5×10^{-2} S cm^{-1} [32].

Argyrodite Type Lithium argyrodite, Li_6PS_5X (with X = Cl, Br, or I), is also one of the sulfide-based Li^+ conductors, having a face-centered cubic lattice of X^-, in which PS_4 tetrahedra locate as if isolated by the anions [31]. Li^+ ions form Li_6S octahedra and distribute over the remaining tetrahedral interstices [31]. In the case of Li_6PS_5Cl and Li_6PS_5Br, the halide ions can partially occupy the place of S^{2-} in the Li_6S octahedra due to an X^-/S^{2-} site disorder, which promote Li^+ mobility significantly. As a result, annealed Li_6PS_5Cl and Li_6PS_5Br exhibit high ionic conductivities of 1.9×10^{-3} S cm^{-1} and 6.8×10^{-3} S cm^{-1}, respectively [36]. In contrast to these, the site disorder does not occur in the case of Li_6PS_5I due to a large size of I^-, and annealed Li_6PS_5I shows the low ionic conductivity of 4.6×10^{-7} S cm^{-1} [36].

$Li_7P_3S_{11}$ Type $Li_7P_3S_{11}$ is glass-ceramic-type sulfide-based electrolytes, which can be obtained through the crystallization of glassy electrolytes formed by a binary mixture of Li_2S–P_2S_5. Binary mixtures of Li_2S–MS_n, such as Li_2S–P_2S_5, Li_2S–B_2S_3, and Li_2S–SiS_2, mixed by a mechanical milling technique exhibit glassy phase with conductivities of 10^{-5}–10^{-4} S cm^{-1} at room temperature. The conductivity can be improved in the order of 10^{-3}–10^{-2} S cm^{-1} by heat treatments because the glassy electrolyte softens and reduces the grain boundary resistance during the crystallization process [36]. Particularly, $Li_7P_3S_{11}$, obtained in 70% Li_2S–30% P_2S_5 in molar ratio, exhibits the ionic conductivity of $\sim 1.7 \times 10^{-2}$ S cm^{-1} [37]. $Li_7P_3S_{11}$ consists of $P_2S_7^{4-}$ di-tetrahedra and slightly distorted PS_4 tetrahedra. An inherent flexibility of readily fluctuating $P_2S_7^{4-}$ polyhedra enables the fast Li^+ migration in the material [48]. The ionic conductivity of $Li_7P_3S_{11}$ phase is higher than those of highly conductive thio-LISICONs, which mainly contain PS_4^{3-} [45].

Overall, sulfide-type ISEs possess considerable high ionic conductivities. However, their drawback is their instability. Several Li_2S–P_2S_5 binary systems are known to generate H_2S upon an exposure to moisture [45]. In addition, at the interface with lithium metal, multiple solid phases including Li_2S, Li_3P, $Li_{17}Ge_4$, and polyphosphide are usually formed, and the most common solution for this problem is the formation of a-SEI on lithium metal [1]. Also, for the cathode side, the formation of a protective layer, so-called a buffer layer, usually based on lithium metal oxide (e.g., $LiNbO_3$, Li_2ZrO_3) or lithium borate (e.g., $Li_3B_{11}O_8$), is effective [1].

10.2.4 Solid Polymer Electrolytes

Non-swollen dry polymer solid electrolytes, so-called SPEs, with suitable physicochemical and mechanical properties can be easily processed into thin separators. The advantages of SPEs as compared to the ISEs are easy fabrication, better scalability, high levels of safety, and flexible shapes. Some polymers with a high polarity, such as poly(ethylene oxide) (PEO) and poly(ethylene carbonate) (PEC), dissolve a large variety of lithium salts, such as lithium triflate ($LiCF_3SO_3$), lithium bis (fluorosulfonyl)imide (LiFSI), and lithium bis(trifluoromethanesulfonyl)imide (LiTFSI). The cations and anions dissociated in the polymer matrices are both mobile, and therefore SPEs act as a dual-ion conductor. Since the ion motion in the polymer matrices is assisted by the segmental motion of polymer chains, it mostly occurs within the amorphous fraction of the polymer matrix above its glass transition temperature (T_g). In this temperature range, the SPEs exhibit an ionic conductivity of around 10^{-3}–10^{-4} S cm^{-1}. To reduce T_g, but to still retain the solid state, copolymerization, insertion of a branch structure, and cross-linking have been undertaken [49]. In addition, the use of inorganic additives such as Al_2O_3-, ZrO_2-, TiO_2-, SiO_2-, and Li^+-conductive ceramic fillers (i.e., ISEs) has been confirmed to improve ionic conductivity and, mainly, enhance the mechanical strength of the resulting polymer membranes [50].

Despite these promising features, many drawbacks hinder the application of SPEs in LMB such as:

1. Small t_{Li+}, generally lower than 0.5
2. Occurrence of lithium dendrite growth and dead lithium formation, leading to poor efficiency and limited reversibility upon cycling
3. Low electrochemical anodic limit, around 4–4.1 V vs. Li^+/Li, that limits the choice of cathode.

Many efforts are presently devoted to tackle these issues. The fixation of an anion structure such as carboxylate, sulfonate, sulfonylimide, etc., onto a polymer backbone allows the SPEs to have the t_{Li+} of unity. In this case, the effective dissociation of the immobilized anions and Li^+ is essential for the ion conduction. Recently, fixation of sulfonylimide on SPEs is dominating the material development because a

delocalized negative charge of the anion is favorable for the ion dissociations [51]. In addition, since an enlarged conjugation structure adjacent to the anion structure can reduce the ionic interactions, several polystyrene derivatives with functional structures at the para position have been designed as Li^+-conductive SPEs [51].

Besides PEO, also PEC has been proposed and demonstrated as a potential polymer matrix having the favorable combination of good physicochemical properties and satisfactory conductivity even at low temperatures. PECs show also a better anodic stability compared to PEO, thus allowing the use of high-voltage cathode such as layered oxides. On the other hand, the mechanical properties of PECs counterbalance the benefits, and relevant dendrite growth occurs at the lithium metal side [52]. In such cases, the use of dual or multiple polymer layers, having different functions, may help the homogeneous lithium metal plating/stripping, thus suppressing the dendrite growth.

10.3 Sodium and Sodium Ion Batteries

10.3.1 Battery Technologies Based on Na Metal

Among the emerging battery technologies alternative to LIBs, sodium-based batteries, in particular sodium metal batteries (NMBs), sodium ion batteries (NIBs), all-solid-state sodium metal battery (ASS-NMB), Na–S, and Na–O_2, show attractive benefits such as sustainable precursors, secure raw material supplies, and, in principle, low costs [53–56].

Figure 10.2 shows a schematic view of the most common Na batteries [55]. NIBs are represented by a porous Na-free negative electrode, a liquid electrolyte, and a Na-rich positive electrode; the full battery is assembled in the discharged state (Fig. 10.2a) like LIBs. The most common negative electrodes are composite films constituted by insertion-type active material, but also conversion and alloying materials have been proposed and tested. On the other side of the battery, the most common positive electrode materials tested successfully are layered ternary oxides that exploit the reversible insertion/de-insertion of Na^+ ions driven by the redox reactions such as Mn^{4+}/Mn^{3+}, Ni^{4+}/Ni^{3+}, or Co^{4+}/Co^{3+}. Regarding liquid electrolytes, formulation closely matching those of LIBs based on organic carbonate solutions has been demonstrated for the utilization in NIBs by simply substituting lithium salts with sodium salts. An appealing advantage of NIBs compared to LIBs is the possible use of Al as the negative electrode's current collector instead of Cu, thanks to the inability of Al to alloy with Na above the Na^+/Na plating/stripping redox potential [57].

ASS-NMBs are based on positive and negative electrodes, like that of NIBs, whereas the electrolyte is a solid composite (Fig. 10.2b). ASS-NMBs are recognized as a promising future battery technology because of their highly improved thermal stability, although there is room for performance improvement. Other advanced systems are Na–O_2 and Na–S batteries. The former exploits the plating/stripping

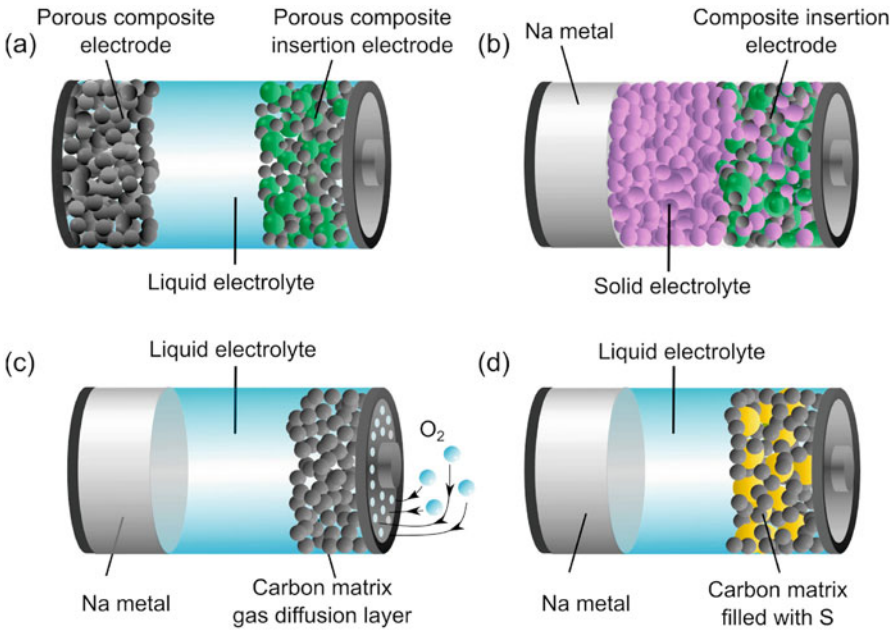

Fig. 10.2 Schematic view of the most common Na battery concepts, (**a**) Na ion battery, (**b**) solid-state Na metal battery, (**c**) Na/O_2, and (**d**) Na/S [55] (License n. 5,396,641,494,902)

reaction of a Na metal at the anode side, whereas porous conducting carbon-based composites in contact with O_2 are used as the cathode, as depicted in Fig. 10.2c. The electrolyte can be either aqueous or aprotic. The latter, Na–S batteries, has very similar configuration compared to Na–O_2 ones, the most relevant difference being the presences of a sulfur–carbon composite at the positive electrode and the exclusive use of either liquid or solid aprotic electrolyte.

This section addresses an overview of state-of-the-art Na batteries, which represent an attractive solution almost suitable to replace Li ion technology in many future applications [53–56].

10.3.2 Toward Sodium Ion Batteries: Cathode Materials

Research on active materials for cathodes in NIBs can take advantages from all similar previous studies for LIBs. Table 10.2 visually summarizes the relative merits of many of the most promising cathodes for NIBs, namely, O3-$NaMO_2$ and P3-Na_xMO_2, Prussian blue analogs (PBA), sodium vanadate phosphates (NVP), and sodium vanadate fluorophosphates (NVPF), belonging to layered oxides (O3-$NaMO_2$ and P3-Na_xMO_2), hybrid materials (PBA), and polyanionic phases (NVP and NVPF) [55, 58–61].

Table 10.2 Comparison of performance for the most promising NIB's cathodes. The different colors of the symbols represent high (green), average (orange), and poor (red) performance. Acronyms of the compounds are described in the main text [55] (License n. 5,396,641,494,902)

Material	O3 $NaMO_2$	P2 Na_xMO_2	PBA	NVP	NVPF
Energy (V/G)					
Rate					
Cost/Sustainability					

Layered Oxides These materials have a two-dimensional layered structure, in which the Na ions intercalate and deintercalate reversibly. The general formula of the most advanced materials within this class is $Na_xMM'M''M'''O_2$, where M, M', M'', and M''' = transition metals, Sn, Al, Mg, etc. This family of materials has a small molecular weight and therefore a large theoretical capacity; their stoichiometries and redox mechanisms are comparable to those of their Li analogs successfully used in LIBs [62]. Differently from the lithium layered oxides, Na ions can be coordinated by both prismatic (P) and octahedral (O) sites in the layered oxide structure, giving rise to a large variety of phases with different transition metals and stacking structures. From the performance point of view, capacities can reach as large as 200 mAh g^{-1} [62, 63]. The most critical drawback of these materials is the anticorrelation between Na content and cycling stability. In fact, materials with a Na/M ratio close to unity show large initial specific capacities but suffer from a remarkable capacity fading. On the other hand, layered phases with Na/M ratios close to 0.7 show excellent stability for prolonged cycling at the expense of the overall capacity [62, 63]. Presently, research efforts are placed on adding extra-capacity to layered phases arising from excess sodium and anionic redox activity. However, true Na-rich phases, i.e., $Na_{1+x}M_{1-x}O_2$, similar to the so-called lithium-rich layered oxides, are still elusive due to dimension of the Na atom, being larger than the Li one.

Polyanionic Compounds Polyanionic compounds are also under study as positive electrodes for NIBs. Their working potentials can be easily tuned by changing the composition of the cations and polyanions in the structure, thanks to the close interplay between the variable intensity of the inductive effect provided by different polyanionic groups and the redox activity of the different transition metals [64, 65]. The most common polyanionic compounds for NIBs crystallize in typical prototype lattices, like tavorite, alluaudite, olivine, and NASICON. The crystalline structure of these materials is more stable compared to layered oxides and allows a full intercalation/de-intercalation of one or two Na ions. The best performances

reported in a full cell are delivered by V^{3+}-containing compounds [65]. In particular, the NASICON-like $Na_3V_2(PO_4)_3$ (NVP) [66] and $Na_3V(PO_4)_2F_3$ (NVPF) in a full cell with hard carbon (HC) as the negative electrode and a liquid aprotic electrolyte can deliver specific capacities as large as 120 mAh g^{-1} at 3.4 V vs. Na^+/Na with a good capacity retention even at high current rates [65, 66].

Prussian Blue Analogs (PBAs) PBAs are very attractive materials for positive electrodes in NIBs. Their general stoichiometry is $A_xM[M'(CN)_6]_{1-y}\bullet zH_2O$, where A is an alkali metal, M and M' are a transition metal ion, and y is the fraction of vacancies in the crystal structure [67, 68]. Like in the case of layered oxides and polyanionic structures, also for PBA the choice of specific transition metal blends allows to tune the redox potential of NIBs [58, 69], allowing the materials to work either as cathode or anode. PBAs have been proposed by the US company Natron that demonstrated the ability of PBAs to operate simultaneously as positive electrodes in the form of sodium hexacyanoferrate and as negative electrodes in the form of hexacyanomanganate, reaching very promising performance [70].

10.3.3 Toward Sodium Ion Batteries: Anode Materials

A visual comparison among the promising materials for negative electrodes in NIBs is summarized in Table 10.3. Materials can be grouped depending on the reaction mechanism upon Na^+ incorporation/de-incorporation: insertion (HC, graphite, TiO_2, Na_xTiO_3), alloying (Sn/C, P/C, Sb/C), conversion (MoS_2/C), and mixed alloy conversion (Sb_2O_3/C).

Insertion Materials The most promising insertion-based materials are the so-called hard carbons (HCs) having their specific capacities in the range of 300–350 mAh g^{-1}, with a Coulombic efficiency in the first cycle as high as 80% [71] and a working potential below 1 V vs. Na^+/Na. On the other hand, soft carbons (SCs) show a much smaller capacity compared to HCs, i.e., 200–250 mAh g^{-1}, but at lower working potential 0.5–0.6 V vs. Na^+/Na. Overall, despite the capacity retention in prolonged

Table 10.3 Comparison of performance for the most promising NIB's anodes. The different colors of the symbols represent high (green), average (orange), and poor (red) performance [55] (License n. 5,396,641,494,902)

Material	Hard Carbon	Graphite	Sn/C	P/C	Sb/C	TiO_2	Na_2TiO_3	MoS_2/C	Sb_2O_3/C
Energy									
Rate									
Cost/Sustainability									

cycling being better for SCs compared to HCs, the latter phases (i.e., HCs) are the most promising active materials due to the much smaller accumulation of irreversible capacity compared to SCs, both in the first cycle and cycle-by-cycle, thus minimizing the waste of charge and the sacrificial positive electrode masses in a full NIB configuration. To improve the performance of HC, two main strategies are presently explored [72]. One is the optimization of the HC microstructure and surface composition to enhance the specific capacity through pseudo-capacitive and pseudo-plating sodium incorporation mechanisms [73, 74], whereas the second one is the incorporation of additional and different sp^2 carbon structures (like SCs or graphene) in HC-based carbon electrodes [75]. Both strategies can increase the capacity unfortunately at the expense of the Coulombic efficiency [75]. Beyond the improvement of performance, keeping sustainability and low environmental impact of these kinds of materials is important because these are critical characteristics. With this respect, it is also crucial to choose the correct precursors for these materials to keep the low costs and the sustainable philosophy of HC [76].

Alloying Materials This type of anode material shows a higher specific capacity compared to HC and operates at low voltages [77]. The alloy-forming materials gain attention due to the ability to incorporate/de-incorporate more than one Na atom per redox atom, but as a trade-off, they suffered from huge volumetric changes upon cycling. Different strategies have been proposed to address this issue, such as minimization of active material particles into a nanometric scale to reduce the mechanical strain per one particle, the formation of core–shell materials to physically restrict the volume change, and the utilization of carbon-based additives as a buffer space [78]. At the same time, however, it is necessary to evaluate whether these improvements are essential from different perspectives. For instance, carbon-based additives are added as stabilizing components for alloy-forming materials, but it also commits as "dead weight" and affects practical capacity of total electrode mass.

The alloy-forming materials are classified into group 4 elements (Si, Ge, Sn), group 5 elements (P, As, Sb, Bi), and their binary or ternary alloys. Among the group 4 elements, Si and Sn are attractive materials because of their abundance. Despite the successes of Si in LIBs, Si has not been that successful in NIBs. In the case of Sn, there are a number of similarities between the Sn in NIBs and LIBs. Among group 5 elements, P is the element with highest theoretical capacity 2596 mAh g^{-1} arising from the formation of Na_3P [79], but due to its high flammability, its practical applications have been hindered [80]. Most of developments are centered on P/carbon composites due to large volume changes during cycling as well as low electric conductivity. P/graphene composites are known to show outstanding performances [81], as well as Sb/carbon composite which can reversibly deliver up to 3 Na per atom and reach a specific capacity of 610 mAh g^{-1} with 95% of capacity retention over 100 cycles [82]. Unfortunately, however, due to the high cost, toxicity, and low sustainability of the latter material, its practical application is not recommended.

Metal Oxides Like in the case of LIBs, a variety of metal oxides have been investigated as anode materials for NIBs, and they are known to show distinctive mechanisms of anode functionality. Among these materials, the most representative

one is titanium oxide, which operates through an insertion mechanism changing its structure from crystalline to amorphous [83]. Despite the high operating voltage and the low Coulombic efficiency, this material is very promising because of the low cost, low toxicity, and availability [83]. Since the conductivity of titanium oxide is low, the use of dopant has been proposed to increase its electronic conductivity. To this end, the materials such as TiO_2 nanosheets/graphene oxide composites have been developed and demonstrated to show a capacity above 175 mAh g^{-1} at 1C for 200 cycles and 90 mAh g^{-1} at 20C for 10,000 cycles [84].

Conversion Materials The reaction of this type of materials with Na is known to form a new phase which is structurally very different from the starting one, specifically $M_aX_b + (bc)\cdot Na \rightleftarrows aM + bNa_cX$, in which M is a metal (Cu, Fe, Sn, etc.) and X is an anion (O, S, P, etc.). Despite their high theoretical capacity, there are different issues related to the conversion materials, such as a low first cycle Coulombic efficiency, an insulating property, a voltage hysteresis, and a large volumetric expansion upon cycling together with consequent electrode degradation in long term due to the deep structural transformation. The electrode composition design and the right choice of the electrolyte are two investigated strategies to improve and solve the issues listed above. MoS_2 represents a typical conversion-type material with a theoretical capacity of about 670 mAh g^{-1} [85]. The electrochemical performance and its stability can be improved by engineering the materials such as the formation of different heterostructures or the combination of MoS_2 layers with different carbon-containing species [86]. Yet, due to the complexity to scale up a controlled synthesis of MoS_2, the large-scale application of this material has not been successful.

New emerging candidates are the metal phosphides [87] because they sustain the conversion reaction of the phosphorus within a metal atom network which provides electric conductivity. Moreover, in these materials, the volumetric expansion and long-term degradation are mitigated [88].

10.3.4 Liquid Electrolytes and SEI Formation in NIBs

In the case of LIBs, there are various standard electrolytes, which are also commercially available. In contrast to this, the optimal electrolyte of NIBs is still under development [89]. Like the electrolytes for LIBs, the performance of electrolytes for NIBs is strongly dependent on the electrode chemistry and electrode combination, making the optimization of an electrolyte composition complex. Especially in the case of NIBs, the ability of electrolyte to form SEI at the anode side is crucial because the SEI based on sodium salts has a higher solubility compared to that based on lithium salts; thus, the SEI undergoes continuous creation and destruction [90].

The main salts used in literature are sodium perchlorate ($NaClO_4$), sodium hexafluorophosphate ($NaPF_6$), sodium triflate ($NaCF_3SO_3$), and sodium bis (trifluoromethanesulfonyl)imide (NaTFSI), which are combined with ether or

carbonate solvents [89]. $NaClO_4$ was chosen in the early stage of NIB research, but it is not ideal because of its explosive nature. As an alternative salt, $NaPF_6$ has been employed most frequently, although its performances are strongly affected by the presence of impurities [91].

The main solvents used together with these salts are the same for LIB technology, such as propylene carbonate (PC), ethylene carbonate (EC), and dimethyl carbonate (DMC), or their mixtures, which are known to form a stable SEI in the case of LIBs [91]. Since, in the case of NIBs, there is a problem in the stability of SEI as mentioned before, the use of additives has been recommended to form a compact, uniform, and more stable SEI, such as FEC and VC [92], which is the same additive used to create m-SEI in LIBs. In addition to these, sodium difluoro(oxalato)borate (NaDFOB), succinonitrile (SN), and 1,3-propane sultone (PS) have been reported as potential additives. It should be noted that in the case of NIBs, also ether-based electrolytes show very good performances for different active materials [93] including high surface carbons [94]. The use of ether-based electrolytes allows the co-intercalation of solvated Na^+ into graphite and enables the formation of stable SEI with enhanced Na plating/stripping efficiency.

Several ionic liquids and aqueous-based electrolytes are also proposed as more sustainable and stable electrolytes [89, 95]. The use of ionic liquids has positive effect on the stability of SEI. Because of this, very promising results have been obtained, for example, when ionic liquids are combined with TiO_2 anode material [96]. Due to the high cost of this class of electrolytes, practical application is not yet realized. In contrast to this, aqueous electrolytes have advantages in terms of their low cost, good sustainability, and safety [60]. However, the structural stability of the electrodes in water and the possible side reactions need to be assessed carefully [60]. Recently, the concept of the "water-in-salt" (WiS) electrolytes has been proposed. This class of electrolytes is defined as the concentrated aqueous solution of salt, in which the number of water molecule per ion is far below the solvation number [60]. These electrolytes consist of contact ion pairs (CIPs) and aggregated cation–anion pairs, which decrease the availability of water and improve its electrochemical stability. By employing the WiS electrolyte, symmetric NIBs based on a dual V^{3+}/Ti^{4+} NASICON-structured $Na_2VTi(PO_4)_3$@C bifunctional electrode were successfully investigated, showing a stable performance over 2500 cycles at 10C [97]. This result demonstrated that the fluorine-rich SEI can suppress the electrode dissolution [97]. Important results of the advances in electrolyte/electrode optimization, related to formulation of advanced electrolyte system, are well summarized in the review of Chen and co-workers [98].

10.3.5 Next-Generation Sodium Batteries

An important step is being taken toward an all-solid-state configuration of the NIB to eliminate the serious problems related to the flammability of liquid electrolytes [99]. The first solid-state sodium ion conductor dates to the 1960s, when a fast

two-dimensional sodium-ion-transport phenomenon was discovered in β-alumina ($Na_2O•11Al_2O_3$). In the same period, NASICON-type compounds were first studied leading to the development of $Na_{1+x}Zr_2Si_xP_{3-x}O_{12}$ ($0 \leq y \leq 3$). Many efforts have been made to elucidate the mechanism of Na^+ transport and to achieve the optimal compositions. Recently, the inclusion of NaF at the synthesis step of NASICON was found to be effective for the fast ion transport (resulting in a conductivity of about 4×10^{-3} S cm^{-1}). In addition, different kinds of solid-state electrolytes have been reported, such as those based on SPEs as well as oxide and sulfide ISEs, as summarized by Zhao et al. [100]. The ionic conductivity and electrochemical stability of Na^+-conductive solid-state electrolytes are still low, and further development is necessary for the commercial use [99].

Other state-of-the-art systems for future sodium technologies are Na–S and Na–O_2 batteries [101]. As a closed system, in this section, focus is placed on Na–S batteries only, but both are promising systems. Na–S batteries were patented by Ford Motor Company in the 1960s, which were made of a β-alumina ceramic electrolyte and cycled at high temperature around 300 °C [102]. At this temperature, Na and S are both molten and need to be separated by the solid electrolyte. For a practical application, the working temperature of Na–S batteries must be reduced, and thus room temperature or intermediate temperature Na–S batteries are being reconsidered [103]. The important difference between Li–S and Na–S batteries is the thermodynamically stable species of alkali metal polysulfides, which should be considered for further development, possibly being both advantageous and disadvantageous.

10.4 Battery Technologies Based on Alkaline Earth Metals

10.4.1 Rechargeable Magnesium Ion Batteries

Magnesium ion batteries (MIBs) have attracted intensive attention due to their high capacity, high security, and low-cost properties. However, the performance of MIBs is seriously hindered by the intense polarization and slow diffusion kinetics of Mg^{2+} ions. To solve these issues, numerous efforts based on both experimental and theoretical studies have been proposed [104, 105]. In this section, the latest advancement in anode and cathode materials as well as electrolytes for MIBs is summarized and discussed.

10.4.1.1 Negative Electrode Materials for MIBs

Metallic Magnesium Anodes The volumetric energy density of Mg is higher than that of Li (3833 vs. 2046 mAh cm^{-3}), which is beneficial for the energy storage systems [106]. Different from the lithium metal, Mg was considered for a long time as a metal whose plating is homogeneous without formation of any dendritic structures [107, 108]. This, together with the low reduction potential of Mg^{2+} (–

2.37 V vs. SHE), makes Mg metal an ideal anode. Despite these merits, recently some authors pointed out the potential hazards related with a formation of dendritic forms or needlelike structures due to uneven deposits on magnesium metal [109–111]. Moreover, surface side reactions are known to occur on the anode side resulting in the accumulation of passivation films during the initial cycles of batteries. Unlike the formation of the SEI on the lithium metal, many reports assume that the passivation layers on the metallic magnesium have low ionic conductivity for magnesium cations [112]. Related to the formation and passivation properties of the interphase, the Coulombic efficiency of magnesium stripping and plating is the most critical parameter, and this is strongly affected by the electrolyte, its chemical properties, purity, and concentration of salt(s). Early generation of nucleophilic electrolytes [113, 114] in ether-based solvents is known to keep magnesium surface at least partially active (non-passivated). Acting on the metal anode itself, Liang et al. synthesized ultrasmall Mg particles with a diameter of ~2.5 nm [115]. The ultrasmall nanoparticles reduced the thickness of the passivation film, which improved the deposition of Mg. Chemical modification is another feasible way to control the reactivity of Mg metal. Lv et al. used a $SnCl_2$–dimethoxyethane (DME) solution to treat Mg foil and obtained a modified Mg anode with a tin-based artificial layer [116]. The Mg anode can maintain stable plating/stripping for more than 4000 cycles at a high current density of 6 mA cm^{-2}. In the same manner, by adding $GeCl_4$ into $Mg(TFSI)_2$–DME electrolyte, the Ge-based artificial layer was also formed on the Mg surface, showing a self-repairing process [117].

Alloying Anodes Some elements from block p are known to electrochemically react with magnesium ions to form an alloy. Alloying materials, such as bismuth (Bi), tin (Sn), and phosphorus (P), are promising alternatives to Mg metal anode [118]. Alloy materials may have synergistic effects in MIBs, bringing new properties that single Mg metal does not have. Bi anode (theoretical volumetric capacity is 3783 mAh cm^{-3}) [119] can rapidly insert and extract Mg^{2+}, with the ion dynamics being related to defect chemistry. In general, gravimetric and volumetric capacities related to the electrochemical alloying are very high (theoretically up to 900 mAh $g^{-1}_{(Sn)}$ and 6570 mAh $cm^{-3}_{(Sn)}$ for the formation of Mg_2Sn). Synergistic effects have been expected by combining multiple elements such as Bi–Sb (solid solution), Bi–Sn (composite), or intermetallic compositions of InBi, SnSb, or InSb [120–122]. Like the alloying-type electrode materials in LIBs, the volumetric changes due to the alloying and de-alloying process hamper the long-term cycling of the electrode. However, with a good electrode formulation, high reversible cycling has been demonstrated especially with Bi-based electrodes (Fig. 10.3) [123]. It is also important to consider that alloy electrodes might be easier to produce than magnesium metal electrode foils. Indeed, alloys can be synthetized in the form of powder by ball-milling or high-temperature reactions, which can be easily integrated in the battery industry. Moreover, alloys are certainly less surface sensitive than magnesium metal and might be of interest for protecting the Mg surface from the dendritic growth.

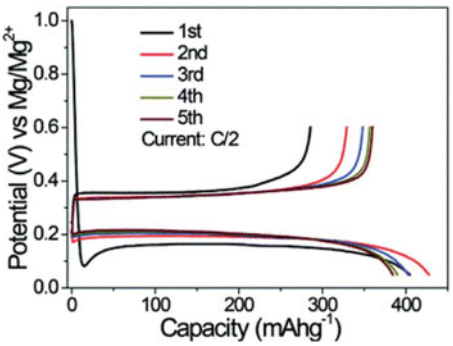

Fig. 10.3 Electrochemical behavior of Bi nanowires in a BilMg half-cell at C/2 with an organohaloaluminate electrolyte [123] (License n. 1,322,765)

Intercalation-Type Anodes Although graphite has been widely employed in conventional LIBs, it is difficult for Mg^{2+} to be inserted into graphite due to its high ionization potential (7.65 eV for Mg and 5.39 eV for Li) [124]. However, Kim et al. proved that the co-intercalation of Mg^{2+} and linear ether solvents is possible through the density functional theory (DFT) calculations [125]. The Mg^{2+} storage properties of carbon nanotubes (CNTs) have also been studied by the DFT. Aslanzadeh et al. studied the influence of CNTs' diameter on the voltage of MIBs by calculating the adsorption energies of zigzag CNTs [126] and demonstrated that the cell voltage increased with the increase of CNTs' diameter. Recently, research interest was shifted to graphene to explore its potential as the anode material for MIBs. Graphene with 25% double-vacancy defects can achieve a Mg^{2+} capacity of 1042 mAh g^{-1} [127]. In addition to these, many other two-dimensional materials have been studied, such as transition metal carbides (MXene) [128] and borides (MBene) [129]. Regarding metal oxide insertion materials, TiO_2 is a very common anode for various secondary batteries. However, the limited capacity of 110 mAh g^{-1} at 0.1 C seriously obstructs its application in MIBs [130]. According to the research of Luo et al., proton charge compensation in Ti-deficient TiO_2 (B) nanowires ensures more thermodynamic feasibility and sufficient intercalation sites for Mg^{2+}, thereby increasing the capacity.

10.4.1.2 Positive Electrode Materials for MIBs

The cathode material, a key component of MIBs, predominantly determines the energy density of batteries. However, most of the cathode materials of MIBs show small capacity and poor rate capability, which seriously hinder the battery performance. Most studies on Mg batteries focus on the combination of Mg metal with inorganic cathodes based on transition metal redox centers. As of today, inorganic oxide, polyanionic, and sulfide compounds are the focus of attention of the research community, but they all present their pros and cons. Moreover, research on inorganic cathodes for magnesium batteries is sometimes quite perplexing as the lack of highly oxidative stable Mg electrolytes prevents the evaluation of Mg insertion reactions at high voltages.

Chevrel Phase Mo_6S_8 Research on the cathode materials for Mg insertion was accelerated by the seminal work of Aurbach et al. with a prototype full Mg cell based on the Chevrel phase Mo_6S_8 [114] and opened a large avenue of research on chalcogenides. These structures are very promising due to the weak electrostatic interactions between Mg^{2+} ions and the sulfide/selenide-based anion framework. The low operating voltage (~1.1 V vs. Mg^{2+}/Mg) and low specific capacity (~100 mAh g^{-1}) of Mo_6S_8, related to an incomplete de-insertion of Mg ions due to the trapping of partial charges at room temperature, are limiting factors for commercial application of the given technology. Substituting sulfur by selenium allows for a 100% capacity usage [131] but at the expense of the specific capacity value. Although the voltage and capacity values are too modest to obtain energy densities competitive with Li ion batteries, Chevrel structures remain the benchmark electrodes for Mg batteries as they offer remarkable insertion/de-insertion kinetics and good reversibility.

Layered Cathode Materials Layer materials possess two-dimensional transmission channels, which enable rapid Mg^{2+} migration. The reported layered cathode materials for MIBs include both transition metal oxides and transition metal sulfides, such as V_2O_5, MnO_2, MoS_2, and TiS_2 [132]. As a representative, V_2O_5 has attracted great attention due to its high theoretical capacity (~295 mAh g^{-1} for MgV_2O_5) and working voltage (~2.35 V vs. Mg^{2+}/Mg). Compared with transition metal oxides, the relatively low ionization degree of S in transition metal sulfide weakens the electrostatic interaction between Mg^{2+} and negative charge, which is favorable for the migration of Mg. Yang et al. studied the diffusion kinetics of Mg^{2+} in MoS_2 (theoretical capacity of 223.2 mAh g^{-1}) [133].

Polyanionic Cathode Materials Polyanionic compounds have been widely used in MIBs because of their versatile variety, stable structure, and strong inductive effect [134]. In $MgMSiO_4$ (M = Mn, Co, Fe, etc.), Mg^{2+} diffuses from the octahedral (O) site to the tetrahedral (T) site [135], with an energy barrier of 740÷770 meV [136]. Despite olivine $FePO_4$ performing well in LIBs, its capacity in MIBs is only ~13 mAh g^{-1} at 20 mA cm^{-2} [137], which can be attributed to the amorphous phase produced on the material surface during the discharge process, preventing Mg^{2+} from entering the bulk phase of $FePO_4$.

Organic Cathode Materials Although inorganic materials have widely dominated the field of rechargeable batteries, a great amount of attention has been recently placed on organic materials because they possess many crucial advantages, like safety, sustainability, green, low cost, and high theoretical capacity [138]. Carbonyl conjugates are a large group possessing many C=O functionalities, essentially determining properties such as diversity, fast reaction kinetics, and high specific volume. Therefore, compared to other types of organic cathode materials, carbonyl-conjugated compounds are expected to develop as the next generation of cathode materials for Mg batteries. Quinone-based monomers are particularly suitable as an active storage unit, and most of recent reports [139] provided highly attractive

properties in terms of energy and power density as well as cyclability. Other reports showed applicability of imides and radical organic compounds [140], which in theory are less attractive in terms of energy density. As well known, electrochemical characteristics depend also on type of electrolyte, where both salts and solvents play important roles [141]. It has been demonstrated that the use of $Mg(TFSI)_2$ salt can increase the capacity utilization of organic electrodes, while the use of $AlCl_3$ can upshift the potential of redox active compounds [142]. Although redox active organics in the form of different polymers show the best properties in terms of cycling and rate capability, there are still some important challenges that need to be addressed before their potential commercialization.

10.4.1.3 Electrolytes for MIBs

To make MIBs commercially available, further breakthroughs in the electrolyte chemistry development are needed. As for other battery technologies, the electrolytes for MIBs should fulfill multiple criteria such as low toxicity, low cost, wide electrochemical stability window, and high ionic conductivity. The following main types of the electrolytes have been explored in MIB technologies: (i) liquid-organic solvent electrolytes, (ii) solid-state electrolytes, (iii) polymer electrolytes, and (iv) ionic liquid-based electrolytes [104].

Liquid electrolytes based on organic solvents or ionic liquids are up to now the best performing materials for Mg deposition/stripping processes. The former electrolytes present a wider electrochemical stability window, while the latter group shows a lower overvoltage in the Mg deposition process, a higher thermal and chemical stability, and a negligible flammability.

For the electrochemical reactivity at the Mg metal anode, even traces of water or other oxygenated coordination ligands must not be present in the electrolyte, to avoid any compromise in the anodic reversibility, cyclability, and current density [143]. Actually, oxygenated species cause the formation of a compact $MgO_x(OH)_y$ layer on the magnesium metal anode, which hinders the anode–electrolyte charge exchange processes promoting on its surface the growth of dendrites. On the other hand, as demonstrated by Novak et al. in the early 1990s [144, 145], water is necessary in the cathodic side to efficiently and reversibly exchange magnesium ions between the solid cathode active material and the electrolyte during insertion and de-insertion processes. This is because water molecules can exfoliate the cathode layered structure and enhance the Mg^{2+} diffusion into the bulk cathode materials by solvating the ions and facilitating their solid-state migration phenomena [146, 147]. Taking all together, developing electrolytes for MIBs able to address the so-called “devil” (at anode) and “holy” (at cathode) water dilemma is a very difficult target.

10.4.2 Calcium Batteries

Calcium (Ca) batteries are emerging as a promising next-generation electrochemical energy storage system, due to the abundant reservation of calcium and the competitive redox potential of Ca^{2+}/Ca. However, the practical realization of rechargeable Ca and Ca ion batteries (CIBs) still relies on the identification of suitable electrodes and electrolytes. Despite reversible calcium plating–stripping being recently demonstrated [148], efforts are still needed to improve both kinetics and efficiency and to allow a wider range of electrolyte formulations. Widening the electrochemical stability window of the electrolyte is crucial to lead the development of positive electrodes operating at high potential [149, 150].

10.4.2.1 The Benefits of Calcium Batteries

Calcium is a divalent alkaline earth metal with an extraordinarily strong oxidative ability in consideration of the −2.87 V vs. SHE redox potential for the Ca^{2+}/Ca couple [151, 152], to be compared to the −3.04 V vs. SHE of the lithium metal electrode. In comparison to other elements under development for battery applications, calcium is the multivalent metal with the most negative redox potential and an ionic radius of 114 pm, very similar to Na^+, that is the cation easily intercalated/deintercalated in/from a variety of materials [153]. The theoretical properties of calcium metal electrodes, in terms of gravimetric and volumetric specific capacities, surpass those of potassium, sodium (both gravimetric and volumetric), and zinc (gravimetric) and are like that of lithium (volumetric), thanks to the favorable combination of intermediate atomic weight and density [149]. In addition, compared to aluminum and magnesium, calcium has a larger ionic radius and a smaller electronegativity [154, 155], thus suggesting on the one hand a lower coordination binding in the liquid phase, thanks to the smaller charge density, and on the other hand a less covalent bonding in solid lattices. Furthermore, it is highly abundant on Earth's crust and industrially inexpensive, much more than Li, Na, K, Mg, and Zn [150, 156, 157]. Even though calcium has an atomic weight seven times larger than lithium, the specific capacities of the calcium-based oxides vary in the 100–250 mAh g^{-1} range, comparable with lithium intercalation positive electrodes, also for what concerns the thermodynamic potentials. Similar to the anode materials available for LIBs, silicon, phosphorus, and carbon negative electrodes can reach large theoretical capacities at relatively low redox potentials also in the case of CIBs. On the other hand, calcium carbide is expected to suffer from large kinetic limitations and overpotentials being the crystal structures of all CaC_2 polymorphs remarkably different from graphite [158]. Moreover, outstanding theoretical performance is achievable for Ca–O_2, as well as for Ca–S, leading to the formation of calcium peroxide and calcium sulfide.

A tentative evaluation of the relative merit of various calcium-based batteries in comparison with LIBs can be made using the theoretical performance of the $LiCoO_2$/C LIB as the baseline (360 Wh kg^{-1}, calculated assuming a $\Delta E^\circ = 3.6$ V and a

specific capacity normalized by the sum of both positive and negative electrode materials) [159]. The CIBs constituted by $CaMn_2O_4$ and Si can disclose a theoretical energy density of about 520 Wh kg^{-1}, being superior to the benchmark LIB (mentioned above) and approaching the desirable figures of the $LiMn_{1.5}Ni_{0.5}O_4$/Si and $LiFePO_4$/Li configurations [159]. Both sulfur battery chemistries, i.e., Ca–S and Li–S, have a comparable theoretical performance (approximately 1800–2000 Wh kg^{-1}) that is, in both cases, exceeded by the Ca–O_2 and Li–O_2 ones (~2400 and ~ 3500 Wh kg^{-1}, respectively).

Overall, calcium-based battery chemistries can theoretically achieve performance of interest, not far from those of lithium-based ones, but research in the field is still in its infancy. To date, the serious exploitation of cathode materials for CIBs just started because of the pioneering work of Ponrouch et al., demonstrating the successful Ca plating/stripping using conventional organic solvents in 2016 [148]. However, the field being in its early stage, the number of reports on positive electrode materials in the literature is still limited [159–165].

10.4.2.2 Challenges in Developing Calcium Batteries

The operating principle of typical calcium batteries is depicted in Fig. 10.4, using inorganic framework as cathode and metallic Ca as anode. In this process, a series of limiting steps occurs [166]. Firstly, the slow diffusion of Ca^{2+} in the positive

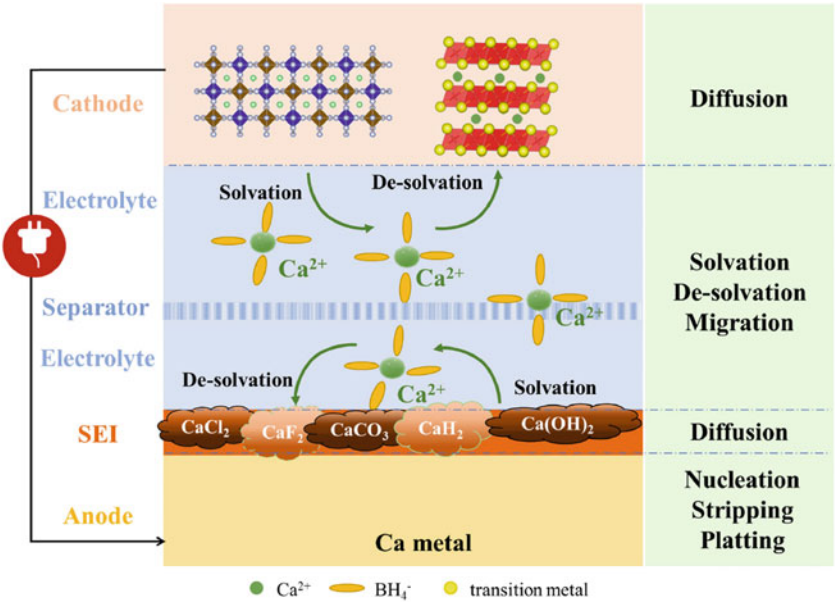

Fig. 10.4 The diffusion, migration process of Ca^{2+} in a typical calcium battery [166] (License n. 5,487,100,248,324)

electrode is inevitable. Although the charge density of Ca^{2+} is small (52 C mm^{-3}, the same as Li^{+}), its diffusion rate is significantly affected by its large ion radius (0.99 Å, compared to 0.76 Å for Li^{+}), which is a dominant limiting factor. Secondly, Ca^{2+} forms solvated calcium in the electrolyte. In some cases, the formed solvated group is relatively large, making it difficult to migrate in the electrolyte. Moreover, when the solvated cluster moves to the electrodes, it needs to be de-solvated. A higher voltage beyond the reorganization energy is needed to break the interatomic bonds in the solvation cluster. This voltage needs to be within the electrochemical stability window of the electrolytes; otherwise, it is easy to decompose the electrolyte. Thirdly, the shuttle of de-solvated calcium ions in SEI is also a matter to be discussed. SEI is a thin film with a thickness of several nanometers between the electrolyte and the anode. This layer can protect the anode from continuous damage and the electrolyte from side reaction with the anode. Ideally, the SEI film is a good ion conductor but needs to be an electronic insulator. As for CIBs, the main components of SEI are $CaCl_2$, $Ca(OH)_2$, $CaCO_3$, CaF_2, CaH_2, etc. [167]. These substances undergo structural changes during the calcium ion diffusion process. Due to the strong interatomic bond, many components are thought to be unable to transmit Ca^{2+} (such as $CaCl_2$, $Ca(OH)_2$, $CaCO_3$, etc.). Also, continuous insertion/de-insertion of Ca^{2+} induces a large volume change of SEI, which may rupture the thin film. Once Ca^{2+} passes the SEI and arrives at the anode, the intercalation, nucleation, or plating of Ca happens [168]. Owing to these complex steps, it is extremely challenging for calcium to deposit.

The main issues and their current state, to be carefully addressed to allow the calcium technology being widely applicable, are summarized as follows:

- The Ca^{2+} ion hosting materials that must be stable enough during the Ca^{2+} diffusion and insertion/de-insertion: Prussian blue analogs, transition metal compounds, and organic compounds are known as potential materials for this requirement [169, 170].
- The reversible stripping/plating of Ca metal at moderate temperature: the proof-of-concept batteries, as of today, showed an average Columbic efficiency of 96% for 50 cycles, which is not sufficient for the practical application [160, 171].
- The efficient solvation/de-solvation process of Ca^{2+}-based electrolytes: different from Li^{+}-based electrolytes, which can form Li^{+}-conducting SEI, the reactions between electrolytes and calcium tend to generate Ca^{2+}-blocking phases when contacting with organic electrolytes [172].

Overall, although great efforts have been made to change the electrolyte and modify the anode–electrolyte interface, the reversible plating/stripping of Ca metal is still tricky and complicated matter. The complexity of working directly with a Ca metal anode drives the search for alternative anodes, which can be categorized into three types based on the calcium ion storage mechanism, including alloying anodes, intercalation anodes, and organic anodes [166, 173], showing the direction toward CIBs.

10.5 Conclusions

Among the emerging battery technologies, Na ion batteries as well as alkali metal batteries, probably solid state, are those expected to become commercially available in the near- (2–5 years) to mid-term (5–10 years) future. Na ion batteries are already being developed by several industries following the CATL announcement made at the end of 2021. Polyvalent metal-based battery chemistries appear to be in the early stage of development with a few hurdles to be addressed in the next few years.

References

1. Varzi A, Thanner K, Scipioni R, Di Lecce D, Hassoun J, Dörfler S, Altheus H, Kaskel S, Prehal C, Freunberger SA (2020) Current status and future perspectives of lithium metal batteries. J Power Sources 480:228803. https://doi.org/10.1016/j.jpowsour.2020.228803
2. Voropaeva DY, Safronova EY, Novikova SA, Yaroslavtsev AB (2022) Recent progress in lithium-ion and lithium metal batteries. Mendeleev Commun 32:287–297. https://doi.org/10.1016/j.mencom.2022.05.001
3. Wang H, Yu Z, Kong X, Kim SC, Boyle DT, Qin J, Bao Z, Cui Y (2022) Liquid electrolyte: the nexus of practical lithium metal batteries. Joule 6:588–616. https://doi.org/10.1016/j.joule.2021.12.018
4. Yuan H, Ding X, Liu T, Nai J, Wang Y, Liu Y, Liu C, Tao X (2022) A review of concepts and contributions in lithium metal anode development. Mater Today 53:173–196. https://doi.org/10.1016/j.mattod.2022.01.015
5. Zhang H, Qi Y (2022) Investigating lithium metal anodes with nonaqueous electrolytes for safe and high-performance batteries. Sustain Energy Fuels 6:954–970. https://doi.org/10.1039/d1se01739j
6. Gao LT, Huang P, Guo Z-S (2022) Critical role of pits in suppressing Li dendrites revealed by continuum mechanics simulation and in situ experiment. J Electrochem Soc 169:060522. https://doi.org/10.1149/1945-7111/ac7668
7. Venturi V, Viswanathan V (2022) Thermodynamic analysis of initial steps for void formation at lithium/solid electrolyte interphase interfaces. ACS Energy Lett 7:1953–1959. https://doi.org/10.1021/acsenergylett.2c00550
8. Zhang S, Yang G, Li X, Li Y, Wang Z, Chen L (2022) Controlled lithium deposition. Front Energy Res 10:837071. https://doi.org/10.3389/fenrg.2022.837071
9. Leung K, Merrill LC, Harrison KL (2022) Galvanic corrosion and electric field in lithium anode passivation films: effects on self-discharge. J Phys Chem C 126:8565–8580. https://doi.org/10.1021/acs.jpcc.1c10602
10. Zhu S, Chen J (2022) Dual strategy with Li-ion solvation and solid electrolyte interphase for high coulombic efficiency of lithium metal anode. Energy Storage Mater 44:48–56. https://doi.org/10.1016/j.ensm.2021.10.007
11. Tewari D, Rangarajan SP, Balbuena PB, Barsukov Y, Mukherjee PP (2020) Mesoscale anatomy of dead lithium formation. J Phys Chem C 124:6502–6511. https://doi.org/10.1021/acs.jpcc.9b11563
12. He D, Lu J, He G, Chen H (2022) Recent advances in solid-electrolyte interphase for Li metal anode. Front Chem 10:916132. https://doi.org/10.3389/fchem.2022.916132

13. Li S, Jiang M, Xie Y, Xu H, Jia J, Li J (2018) Developing high-performance lithium metal anode in liquid electrolytes: challenges and Progress. Adv Mater 30:1706375. https://doi.org/10.1002/adma.201706375
14. Mogi R, Inaba M, Jeong S-K, Iriyama Y, Abe T, Ogumi Z (2002) Effects of some organic additives on lithium deposition in propylene carbonate. J Electrochem Soc 149:A1578. https://doi.org/10.1149/1.1516770
15. Dong L, Liu Y, Chen D, Han Y, Ji Y, Liu J, Yuan B, Dong Y, Li Q, Zhou S, Zhong S, Liang Y, Yang M, Yang C, He W (2022) Stabilization of high-voltage lithium metal batteries using a sulfone-based electrolyte with bi-electrode affinity and $LiSO_2F$-rich interphases. Energy Storage Mater 44:527–536. https://doi.org/10.1016/j.ensm.2021.10.045
16. Wu D, He J, Liu J, Wu M, Qi S, Wang H, Huang J, Li F, Tang D, Ma J (2022) Li_2CO_3/LiF-rich Heterostructured solid electrolyte interphase with superior Lithiophilic and Li^+-transferred characteristics via adjusting electrolyte additives. Adv Energy Mater 12:2200337. https://doi.org/10.1002/aenm.202200337
17. Lu Y, Tu Z, Shu J, Archer LA (2015) Stable lithium electrodeposition in salt-reinforced electrolytes. J Power Sources 279:413–418. https://doi.org/10.1016/j.jpowsour.2015.01.030
18. Li NW, Yin YX, Yang CP, Guo YG (2016) An artificial solid electrolyte interphase layer for stable lithium metal anodes. Adv Mater 28:1853–1858. https://doi.org/10.1002/adma.201504526
19. Niu J, Wang M, Cao T, Cheng X, Wu R, Liu H, Zhang Y, Liu X (2021) Li metal coated with Li3PO4 film via atomic layer deposition as battery anode. Ionics 27:2445–2454. https://doi.org/10.1007/s11581-021-04030-z
20. Wang W, Yuan Y, Wang J, Zhang Y, Liao C, Mu X, Sheng H, Kan Y, Song L, Hu Y (2019) Enhanced electrochemical and safety performance of lithium metal batteries enabled by the atom layer deposition on PVDF-HFP separator. ACS Appl Energy Mater 2:4167–4174. https://doi.org/10.1021/acsaem.9b00383
21. Yao Z, Kang Y, Hou M, Huang J, Zhang J, Yang B, Dai Y, Liang F (2022) Promoting homogeneous interfacial Li^+ migration by using a facile N2 plasma strategy for all-solid-state lithium-metal batteries. Adv Funct Mater 32:2111919. https://doi.org/10.1002/adfm.202111919
22. Fan L, Zhuang HL, Gao L, Lu Y, Archer LA (2017) Regulating Li deposition at artificial solid electrolyte interphases. J Mater Chem A 5:3483–3492. https://doi.org/10.1039/c6ta10204b
23. Ma L, Kim MS, Archer LA (2017) Stable artificial solid electrolyte interphases for lithium batteries. Chem Mater 29:4181–4189. https://doi.org/10.1021/acs.chemmater.6b03687
24. Jin C, Sheng O, Luo J, Yuan H, Fang C, Zhang W, Huang H, Gan Y, Xia Y, Liang C, Zhang J, Tao X (2017) 3D lithium metal embedded within lithiophilic porous matrix for stable lithium metal batteries. Nano Energy 37:177–186. https://doi.org/10.1016/j.nanoen.2017.05.015
25. Lu Z, Zhang Z, Chen X, Chen Q, Ren F, Wang M, Wu S, Peng Z, Wang D, Ye J (2018) Improving Li anode performance by a porous 3D carbon paper host with plasma assisted sponge carbon coating. Energy Storage Mater 11:47–56. https://doi.org/10.1016/j.ensm.2017.09.011
26. Qi LY, Shang L, Chen X, Ye L, Zhang W, Feng P, Zou W, Cao N, Zhou HH, Weitz DA, Li X (2018) A versatile strategy to fabricate 3D conductive frameworks for lithium metal anodes. Adv Mater Interfaces 5:1800807. https://doi.org/10.1002/admi.201800807
27. Raj V, Aetukuri NPB, Nanda J (2022) Solid state lithium metal batteries – issues and challenges at the lithium-solid electrolyte interface. Curr Opin Solid State Mater Sci 26:100999. https://doi.org/10.1016/j.cossms.2022.100999
28. Fan L, Wei S, Li S, Li Q, Lu Y (2018) Recent Progress of the solid-state electrolytes for high-energy metal-based batteries. Adv Energy Mater 8:1702657. https://doi.org/10.1002/aenm.201702657
29. Zhang Z, Shao Y, Lotsch B, Hu Y-S, Li H, Janek J, Nazar LF, Nan C-W, Maier J, Armand M, Chen L (2018) New horizons for inorganic solid state ion conductors. Energy Environ Sci 11:1945–1976. https://doi.org/10.1039/c8ee01053f

30. Manthiram A, Yu X, Wang S (2017) Lithium battery chemistries enabled by solid-state electrolytes. Nat Rev Mater 2:16103. https://doi.org/10.1038/natrevmats.2016.103
31. Bachman JC, Muy S, Grimaud A, Chang HH, Pour N, Lux SF, Paschos O, Maglia F, Lupart S, Lamp P, Giordano L, Shao-Horn Y (2016) Inorganic solid-state electrolytes for lithium batteries: mechanisms and properties governing ion conduction. Chem Rev 116:140–162. https://doi.org/10.1021/acs.chemrev.5b00563
32. Chen R, Li Q, Yu X, Chen L, Li H (2020) Approaching practically accessible solid-state batteries: stability issues related to solid electrolytes and interfaces. Chem Rev 120:6820–6877. https://doi.org/10.1021/acs.chemrev.9b00268
33. Hou M, Liang F, Chen K, Dai Y, Xue D (2020) Challenges and perspectives of NASICON-type solid electrolytes for all-solid-state lithium batteries. Nanotechnology 31:132003. https://doi.org/10.1088/1361-6528/ab5be7
34. Matsui M, Takahashi K, Sakamoto K, Hirano A, Takeda Y, Yamamoto O, Imanishi N (2014) Phase stability of a garnet-type lithium ion conductor $Li_7La_3Zr_2O_{12}$. J Chem Soc Dalton Trans 43:1019–1024. https://doi.org/10.1039/c3dt52024b
35. Xu L, Li J, Deng W, Shuai H, Li S, Xu Z, Li J, Hou H, Peng H, Zou G, Ji X (2020) Garnet solid electrolyte for advanced all-solid-state Li batteries. Adv Energy Mater 11:2000648. https://doi.org/10.1002/aenm.202000648
36. Lian P-J, Zhao B-S, Zhang L-Q, Xu N, Wu M-T, Gao X-P (2019) Inorganic sulfide solid electrolytes for all-solid-state lithium secondary batteries. J Mater Chem A 7:20540–20557. https://doi.org/10.1039/c9ta04555d
37. Chang D, Oh K, Kim SJ, Kang K (2018) Super-ionic conduction in solid-state $Li_7P_3S_{11}$-type Sulfide electrolytes. Chem Mater 30:8764–8770. https://doi.org/10.1021/acs.chemmater.8b03000
38. Avdeev M (2021) Crystal chemistry of NaSICONs: ideal framework, distortion, and connection to properties. Chem Mater 33:7620–7632. https://doi.org/10.1021/acs.chemmater.1c02695
39. Jin Y, Zong X, Zhang X, Liu C, Li D, Jia Z, Li G, Zhou X, Wei J, Xiong Y (2021) Interface regulation enabling three-dimensional $Li_{1.3}Al_{0.3}Ti_{1.7}(PO_4)_3$-reinforced composite solid electrolyte for high-performance lithium batteries. J Power Sources 501:230027. https://doi.org/10.1016/j.jpowsour.2021.230027
40. Ramakumar S, Deviannapoorani C, Dhivya L, Shankar LS, Murugan R (2017) Lithium garnets: synthesis, structure, Li^+ conductivity, Li^+ dynamics and applications. Prog Mater Sci 88:325–411. https://doi.org/10.1016/j.pmatsci.2017.04.007
41. Fuchs T, Mogwitz B, Otto SK, Passerini S, Richter FH, Janek J (2021) Working principle of an ionic liquid interlayer during Pressureless lithium stripping on $Li_{6.25}Al_{0.25}La_3Zr_2O_{12}$ (LLZO) garnet-type solid electrolyte. Batter Supercaps 4:1145–1155. https://doi.org/10.1002/batt.202100015
42. Liu Z, Borodin A, Endres F (2021) Ionic liquid and polymer coated garnet solid electrolytes for high-energy solid-state lithium metal batteries. Energ Technol 10:2100907. https://doi.org/10.1002/ente.202100907
43. Mauger A, Julien CM (2021) Remedies to avoid failure mechanisms of lithium-metal anode in Li-ion batteries. Inorganics 10:5. https://doi.org/10.3390/inorganics10010005
44. Symington AR, Molinari M, Dawson JA, Statham JM, Purton J, Canepa P, Parker SC (2021) Elucidating the nature of grain boundary resistance in lithium lanthanum titanate. J Mater Chem A 9:6487–6498. https://doi.org/10.1039/d0ta11539h
45. Zheng F, Kotobuki M, Song S, Lai MO, Lu L (2018) Review on solid electrolytes for all-solid-state lithium-ion batteries. J Power Sources 389:198–213. https://doi.org/10.1016/j.jpowsour.2018.04.022
46. Lau J, DeBlock RH, Butts DM, Ashby DS, Choi CS, Dunn BS (2018) Sulfide solid electrolytes for lithium battery applications. Adv Energy Mater 8:1800933. https://doi.org/10.1002/aenm.201800933

47. Tao B, Ren C, Li H, Liu B, Jia X, Dong X, Zhang S, Chang H (2022) Thio-/LISICON and LGPS-type solid electrolytes for all-solid-state lithium-ion batteries. Adv Funct Mater 32: 2203551. https://doi.org/10.1002/adfm.202203551
48. Wenzel S, Weber DA, Leichtweiss T, Busche MR, Sann J, Janek J (2016) Interphase formation and degradation of charge transfer kinetics between a lithium metal anode and highly crystalline $Li_7P_3S_{11}$ solid electrolyte. Solid State Ionics 286:24–33. https://doi.org/10.1016/j.ssi.2015.11.034
49. Wang J, Li S, Zhao Q, Song C, Xue Z (2020) Structure code for advanced polymer electrolyte in lithium-ion batteries. Adv Funct Mater 31:2008208. https://doi.org/10.1002/adfm.202008208
50. Mauger A, Julien CM (2022) Solid polymer electrolytes for lithium batteries: a tribute to Michel Armand. Inorganics 10:110. https://doi.org/10.3390/inorganics10080110
51. Zhu J, Zhang Z, Zhao S, Westover AS, Belharouak I, Cao PF (2021) Single-ion conducting polymer electrolytes for solid-state lithium–metal batteries: design, performance, and challenges. Adv Energy Mater 11:2003836. https://doi.org/10.1002/aenm.202003836
52. Wang Y, Chen S, Li Z, Peng C, Li Y, Feng W (2022) In-situ generation of fluorinated polycarbonate copolymer solid electrolytes for high-voltage Li-metal batteries. Energy Storage Mater 45:474–483. https://doi.org/10.1016/j.ensm.2021.12.004
53. Nayak PK, Yang L, Brehm W, Adelhelm P (2018) From lithium-ion to sodium-ion batteries: advantages, challenges, and surprises. Angew Chem 57:102–120. https://doi.org/10.1002/anie.201703772
54. Vaalma C, Buchholz D, Weil M, Passerini S (2018) A cost and resource analysis of sodium-ion batteries. Nat Rev Mater 3:18013. https://doi.org/10.1038/natrevmats.2018.13
55. Hasa I, Mariyappan S, Saurel D, Adelhelm P, Koposov AY, Masquelier C, Croguennec L, Casas-Cabanas M (2021) Challenges of today for Na-based batteries of the future: from materials to cell metrics. J Power Sources 482:228872. https://doi.org/10.1016/j.jpowsour.2020.228872
56. Mohan I, Raj A, Shubham K, Lata DB, Mandal S, Kumar S (2022) Potential of potassium and sodium-ion batteries as the future of energy storage: recent progress in anodic materials. J Energy Storage 55:105625. https://doi.org/10.1016/j.est.2022.105625
57. Murray JL (1983) The Al−Na (Aluminum-sodium) system. Bull Alloy Phase Diagr 4:407–410. https://doi.org/10.1007/bf02868094
58. Peng J, Zhang W, Liu Q, Wang J, Chou S, Liu H, Dou S (2022) Prussian blue analogues for sodium-ion batteries: past, present, and future. Adv Mater 34:2108384. https://doi.org/10.1002/adma.202108384
59. Chang YX, Yu L, Xing X, Guo YJ, Xie ZY, Xu S (2022) Ion substitution strategy of manganese-based layered oxide cathodes for advanced and low-cost sodium ion batteries. Chem Rec 22:202200122. https://doi.org/10.1002/tcr.202200122
60. Zhang H, Tan X, Li H, Passerini S, Huang W (2021) Assessment and progress of polyanionic cathodes in aqueous sodium batteries. Energy Environ Sci 14:5788–5800. https://doi.org/10.1039/d1ee01392k
61. Hwang JY, Myung ST, Sun YK (2017) Sodium-ion batteries: present and future. Chem Soc Rev 46:3529–3614. https://doi.org/10.1039/c6cs00776g
62. Rudola A, Rennie AJR, Heap R, Meysami SS, Lowbridge A, Mazzali F, Sayers R, Wright CJ, Barker J (2021) Commercialisation of high energy density sodium-ion batteries: Faradion's journey and outlook. J Mater Chem A 9:8279–8302. https://doi.org/10.1039/d1ta00376c
63. Yao H-R, Zheng L, Xin S, Guo Y-G (2022) Air-stability of sodium-based layered-oxide cathode materials. Sci China Chem 65:1076–1087. https://doi.org/10.1007/s11426-022-1257-8
64. Jin T, Li H, Zhu K, Wang PF, Liu P, Jiao L (2020) Polyanion-type cathode materials for sodium-ion batteries. Chem Soc Rev 49:2342–2377. https://doi.org/10.1039/c9cs00846b

65. Park S, Chotard J-N, Carlier D, Moog I, Duttine M, Fauth F, Iadecola A, Croguennec L, Masquelier C (2022) An asymmetric sodium extraction/insertion mechanism for the Fe/V-mixed NASICON $Na_4FeV(PO_4)_3$. Chem Mater 34:4142–4152. https://doi.org/10.1021/acs.chemmater.2c00501
66. Jian Z, Han W, Lu X, Yang H, Hu Y-S, Zhou J, Zhou Z, Li J, Chen W, Chen D, Chen L (2013) Superior electrochemical performance and storage mechanism of $Na_3V_2(PO_4)_3$ cathode for room-temperature sodium-ion batteries. Adv Energy Mater 3:156–160. https://doi.org/10.1002/aenm.201200558
67. Li WJ, Han C, Cheng G, Chou SL, Liu HK, Dou SX (2019) Chemical properties, structural properties, and energy storage applications of Prussian blue analogues. Small 15:e1900470. https://doi.org/10.1002/smll.201900470
68. Liu Q, Hu Z, Chen M, Zou C, Jin H, Wang S, Chou SL, Liu Y, Dou SX (2020) The cathode choice for commercialization of sodium-ion batteries: layered transition metal oxides versus Prussian blue Analogs. Adv Funct Mater 30:1909530. https://doi.org/10.1002/adfm.201909530
69. Firouzi A, Qiao R, Motallebi S, Valencia CW, Israel HS, Fujimoto M, Wray LA, Chuang YD, Yang W, Wessells CD (2018) Monovalent manganese based anodes and co-solvent electrolyte for stable low-cost high-rate sodium-ion batteries. Nat Commun 9:861. https://doi.org/10.1038/s41467-018-03257-1
70. Wessells CD (2019) Advances in prussian blue batteries for behind-the-meter applications. ECS meeting abstracts MA2019-03:63. https://doi.org/10.1149/MA2019-03/1/63/meta
71. Kamiyama A, Kubota K, Igarashi D, Youn Y, Tateyama Y, Ando H, Gotoh K, Komaba S (2021) MgO-template synthesis of extremely high capacity hard carbon for Na-ion battery. Angew Chem 60:5114–5120. https://doi.org/10.1002/anie.202013951
72. Saurel D, Orayech B, Xiao B, Carriazo D, Li X, Rojo T (2018) From charge storage mechanism to performance: a roadmap toward high specific energy sodium-ion batteries through carbon anode optimization. Adv Energy Mater 8:1703268. https://doi.org/10.1002/aenm.201703268
73. Li Z, Bommier C, Chong ZS, Jian Z, Surta TW, Wang X, Xing Z, Neuefeind JC, Stickle WF, Dolgos M, Greaney PA, Ji X (2017) Mechanism of Na-Ion storage in hard carbon anodes revealed by heteroatom doping. Adv Energy Mater 7:1602894. https://doi.org/10.1002/aenm.201602894
74. Qiu S, Xiao L, Sushko ML, Han KS, Shao Y, Yan M, Liang X, Mai L, Feng J, Cao Y, Ai X, Yang H, Liu J (2017) Manipulating adsorption–insertion mechanisms in nanostructured carbon materials for high-efficiency sodium ion storage. Adv Energy Mater 7:1700403. https://doi.org/10.1002/aenm.201700403
75. Lin Z, Xiong X, Zheng J, Wang G, Yang C (2017) Three-dimensional N-doped graphene as anode material with superior cycle stability for sodium ion batteries. Mater Lett 202:123–126. https://doi.org/10.1016/j.matlet.2017.05.046
76. Peters J, Peña Cruz A, Weil M (2019) Exploring the economic potential of sodium-ion batteries. Batteries 5:10. https://doi.org/10.3390/batteries5010010
77. Fang L, Bahlawane N, Sun W, Pan H, Xu BB, Yan M, Jiang Y (2021) Conversion-alloying anode materials for sodium ion batteries. Small 17:2101137. https://doi.org/10.1002/smll.202101137
78. Jing WT, Yang CC, Jiang Q (2020) Recent progress on metallic Sn- and Sb-based anodes for sodium-ion batteries. J Mater Chem A 8:2913–2933. https://doi.org/10.1039/c9ta11782b
79. Li WJ, Chou SL, Wang JZ, Liu HK, Dou SX (2013) Simply mixed commercial red phosphorus and carbon nanotube composite with exceptionally reversible sodium-ion storage. Nano Lett 13:5480–5484. https://doi.org/10.1021/nl403053v
80. Ni J, Li L, Lu J (2018) Phosphorus: An anode of choice for sodium-ion batteries. ACS Energy Lett 3:1137–1144. https://doi.org/10.1021/acsenergylett.8b00312

81. Zhang Y, Xia X, Liu B, Deng S, Xie D, Liu Q, Wang Y, Wu J, Wang X, Tu J (2019) Multiscale graphene-based materials for applications in sodium ion batteries. Adv Energy Mater 9:1803342. https://doi.org/10.1002/aenm.201803342
82. Qian J, Chen Y, Wu L, Cao Y, Ai X, Yang H (2012) High capacity Na-storage and superior cyclability of nanocomposite Sb/C anode for Na-ion batteries. Chem Commun 48:7070–7072. https://doi.org/10.1039/c2cc32730a
83. Greco G, Mazzio KA, Dou X, Gericke E, Wendt R, Krumrey M, Passerini S (2019) Structural study of carbon-coated TiO2 Anatase nanoparticles as high-performance anode materials for Na-Ion batteries. ACS Appl Energy Mater 2:7142–7151. https://doi.org/10.1021/acsaem.9b01101
84. Zhang R, Wang Y, Zhou H, Lang J, Xu J, Xiang Y, Ding S (2018) Mesoporous TiO_2 nanosheets anchored on graphene for ultra long life Na-ion batteries. Nanotechnology 29:225401. https://doi.org/10.1088/1361-6528/aab562
85. Wu Y, Zhang C, Zhao H, Lei Y (2021) Recent advances in ferromagnetic metal sulfides and selenides as anodes for sodium- and potassium-ion batteries. J Mater Chem A 9:9506–9534. https://doi.org/10.1039/d1ta00831e
86. Li Y, Liang Y, Robles Hernandez FC, Deog Yoo H, An Q, Yao Y (2015) Enhancing sodium-ion battery performance with interlayer-expanded MoS_2–PEO nanocomposites. Nano Energy 15:453–461. https://doi.org/10.1016/j.nanoen.2015.05.012
87. Xia Q, Li W, Miao Z, Chou S, Liu H (2017) Phosphorus and phosphide nanomaterials for sodium-ion batteries. Nano Res 10:4055–4081. https://doi.org/10.1007/s12274-017-1671-7
88. Li Q, Yang D, Chen H, Lv X, Jiang Y, Feng Y, Rui X, Yu Y (2021) Advances in metal phosphides for sodium-ion batteries. SusMat 1:359–392. https://doi.org/10.1002/sus2.19
89. Eshetu GG, Elia GA, Armand M, Forsyth M, Komaba S, Rojo T, Passerini S (2020) Electrolytes and interphases in sodium-based rechargeable batteries: recent advances and perspectives. Adv Energy Mater 10:2000093. https://doi.org/10.1002/aenm.202000093
90. Mogensen R, Brandell D, Younesi R (2016) Solubility of the solid electrolyte interphase (SEI) in sodium ion batteries. ACS Energy Lett 1:1173–1178. https://doi.org/10.1021/acsenergylett.6b00491
91. Kubota K, Komaba S (2015) Review—practical issues and future perspective for Na-ion batteries. J Electrochem Soc 162:A2538–A2550. https://doi.org/10.1149/2.0151514jes
92. Komaba S, Ishikawa T, Yabuuchi N, Murata W, Ito A, Ohsawa Y (2011) Fluorinated ethylene carbonate as electrolyte additive for rechargeable Na batteries. ACS Appl Mater Interfaces 3:4165–4168. https://doi.org/10.1021/am200973k
93. Palaniselvam T, Goktas M, Anothumakkool B, Sun YN, Schmuch R, Zhao L, Han BH, Winter M, Adelhelm P (2019) Sodium storage and electrode dynamics of tin–carbon composite electrodes from bulk precursors for sodium-ion batteries. Adv Funct Mater 29:1900790. https://doi.org/10.1002/adfm.201900790
94. Zhang J, Wang D-W, Lv W, Zhang S, Liang Q, Zheng D, Kang F, Yang Q-H (2017) Achieving superb sodium storage performance on carbon anodes through an ether-derived solid electrolyte interphase. Energy Environ Sci 10:370–376. https://doi.org/10.1039/c6ee03367a
95. Giffin GA (2016) Ionic liquid-based electrolytes for "beyond lithium" battery technologies. J Mater Chem A 4:13378–13389. https://doi.org/10.1039/c6ta05260f
96. Wu L, Moretti A, Buchholz D, Passerini S, Bresser D (2016) Combining ionic liquid-based electrolytes and nanostructured anatase TiO_2 anodes for intrinsically safer sodium-ion batteries. Electrochim Acta 203:109–116. https://doi.org/10.1016/j.electacta.2016.03.124
97. Shen L, Yang H, Jiang Y, Ma J, Sun T, Zhang M, Zhu N (2021) NASICON-structured $Na_2VTi(PO_4)_3$@C for symmetric aqueous rechargeable Na-Ion batteries with long lifespan. ACS Sustain Chem Eng 9:3490–3497. https://doi.org/10.1021/acssuschemeng.0c07755
98. Huang Y, Zhao L, Li L, Xie M, Wu F, Chen R (2019) Electrolytes and electrolyte/electrode interfaces in sodium-ion batteries: from scientific research to practical application. Adv Mater 31:1808393. https://doi.org/10.1002/adma.201808393

99. Wu JF, Zhang R, Fu QF, Zhang JS, Zhou XY, Gao P, Xu CH, Liu J, Guo X (2020) Inorganic solid electrolytes for all-solid-state sodium batteries: fundamentals and strategies for battery optimization. Adv Funct Mater 31:2008165. https://doi.org/10.1002/adfm.202008165
100. Zhao C, Liu L, Qi X, Lu Y, Wu F, Zhao J, Yu Y, Hu Y-S, Chen L (2018) Solid-State Sodium Batteries. Adv Energy Mater 8:1703012. https://doi.org/10.1002/aenm.201703012
101. Hartmann P, Bender CL, Vracar M, Durr AK, Garsuch A, Janek J, Adelhelm P (2013) A rechargeable room-temperature sodium superoxide (NaO_2) battery. Nat Mater 12:228–232. https://doi.org/10.1038/nmat3486
102. Kummer J, Weber N (1967) A sodium-Sulfur secondary battery. Proc Ann Power Sources Conf 19:113–115. https://doi.org/10.4271/670179
103. Eng AYS, Kumar V, Zhang Y, Luo J, Wang W, Sun Y, Li W, Seh ZW (2021) Room-temperature sodium–sulfur batteries and beyond: realizing practical high energy systems through anode, cathode, and electrolyte engineering. Adv Energy Mater 11:2003493. https://doi.org/10.1002/aenm.202003493
104. Dominko R, Bitenc J, Berthelot R, Gauthier M, Pagot G, Di Noto V (2020) Magnesium batteries: current picture and missing pieces of the puzzle. J Power Sources 478:229027. https://doi.org/10.1016/j.jpowsour.2020.229027
105. Wu X, Dou Y, Lian R, Wang Y, Wei Y (2022) Understanding rechargeable magnesium ion batteries via first-principles computations: a comprehensive review. Energy Storage Mater 48: 344–355. https://doi.org/10.1016/j.ensm.2022.03.039
106. Yoo HD, Shterenberg I, Gofer Y, Gershinsky G, Pour N, Aurbach D (2013) Mg rechargeable batteries: an on-going challenge. Energy Environ Sci 6:2265–2279. https://doi.org/10.1039/c3ee40871j
107. Aurbach D, Cohen Y, Moshkovich M (2001) The study of reversible magnesium deposition by in situ scanning Tunneling microscopy. Electrochem Solid-State Lett 4:A113. https://doi.org/10.1149/1.1379828
108. Matsui M (2011) Study on electrochemically deposited Mg metal. J Power Sources 196:7048–7055. https://doi.org/10.1016/j.jpowsour.2010.11.141
109. Ding MS, Diemant T, Behm RJ, Passerini S, Giffin GA (2018) Dendrite growth in Mg metal cells containing Mg(TFSI)2/Glyme electrolytes. J Electrochem Soc 165:A1983–A1990. https://doi.org/10.1149/2.1471809jes
110. Davidson R, Verma A, Santos D, Hao F, Fincher C, Xiang S, Van Buskirk J, Xie K, Pharr M, Mukherjee PP, Banerjee S (2018) Formation of magnesium dendrites during electrodeposition. ACS Energy Lett 4:375–376. https://doi.org/10.1021/acsenergylett.8b02470
111. Bitenc J, Pirnat K, Žagar E, Randon-Vitanova A, Dominko R (2019) Effect of salts on the electrochemical performance of Mg metal–organic battery. J Power Sources 430:90–94. https://doi.org/10.1016/j.jpowsour.2019.04.114
112. Son SB, Gao T, Harvey SP, Steirer KX, Stokes A, Norman A, Wang C, Cresce A, Xu K, Ban C (2018) An artificial interphase enables reversible magnesium chemistry in carbonate electrolytes. Nat Chem 10:532–539. https://doi.org/10.1038/s41557-018-0019-6
113. Gregory TD, Hoffman RJ, Winterton RC (2019) Nonaqueous electrochemistry of magnesium: applications to energy storage. J Electrochem Soc 137:775–780. https://doi.org/10.1149/1.2086553
114. Aurbach D, Lu Z, Schechter A, Gofer Y, Gizbar H, Turgeman R, Cohen Y, Moshkovich M, Levi E (2000) Prototype systems for rechargeable magnesium batteries. Nature 407:724–727. https://doi.org/10.1038/35037553
115. Liang Y, Feng R, Yang S, Ma H, Liang J, Chen J (2011) Rechargeable Mg batteries with graphene-like MoS_2 cathode and ultrasmall Mg nanoparticle anode. Adv Mater 23:640–643. https://doi.org/10.1002/adma.201003560
116. Lv R, Guan X, Zhang J, Xia Y, Luo J (2020) Enabling Mg metal anodes rechargeable in conventional electrolytes by fast ionic transport interphase. Natl Sci Rev 7:333–341. https://doi.org/10.1093/nsr/nwz157

117. Zhang J, Guan X, Lv R, Wang D, Liu P, Luo J (2020) Rechargeable Mg metal batteries enabled by a protection layer formed in vivo. Energy Storage Mater 26:408–413. https://doi.org/10.1016/j.ensm.2019.11.012
118. Niu J, Zhang Z, Aurbach D (2020) Alloy anode materials for rechargeable Mg ion batteries. Adv Energy Mater 10:2000697. https://doi.org/10.1002/aenm.202000697
119. Kravchyk KV, Piveteau L, Caputo R, He M, Stadie NP, Bodnarchuk MI, Lechner RT, Kovalenko MV (2018) Colloidal bismuth nanocrystals as a model anode material for rechargeable mg-ion batteries: atomistic and mesoscale insights. ACS Nano 12:8297–8307. https://doi.org/10.1021/acsnano.8b03572
120. Blondeau L, Foy E, Khodja H, Gauthier M (2018) Unexpected behavior of the InSb alloy in Mg-Ion batteries: unlocking the reversibility of Sb. J Phys Chem C 123:1120–1126. https://doi.org/10.1021/acs.jpcc.8b10913
121. Niu J, Yin K, Gao H, Song M, Ma W, Peng Z, Zhang Z (2019) Composition- and size-modulated porous bismuth-tin biphase alloys as anodes for advanced magnesium ion batteries. Nanoscale 11:15279–15288. https://doi.org/10.1039/c9nr05399a
122. Song M, Niu J, Yin K, Gao H, Zhang C, Ma W, Luo F, Peng Z, Zhang Z (2019) Self-supporting, eutectic-like, nanoporous biphase bismuth-tin film for high-performance magnesium storage. Nano Res 12:801–808. https://doi.org/10.1007/s12274-019-2291-1
123. Liu Z, Lee J, Xiang G, Glass HF, Keyzer EN, Dutton SE, Grey CP (2017) Insights into the electrochemical performances of Bi anodes for Mg ion batteries using ^{25}Mg solid state NMR spectroscopy. Chem Commun 53:743–746. https://doi.org/10.1039/c6cc08430c
124. Kawaguchi M, Kurasaki A (2012) Intercalation of magnesium into a graphite-like layered material of composition BC_2N. Chem Commun 48:6897–6899. https://doi.org/10.1039/c2cc31435e
125. Kim D-M, Jung SC, Ha S, Kim Y, Park Y, Ryu JH, Han Y-K, Lee KT (2018) Cointercalation of Mg^{2+} ions into graphite for magnesium-ion batteries. Chem Mater 30:3199–3203. https://doi.org/10.1021/acs.chemmater.8b00288
126. Aslanzadeh SA (2020) A computational study on the potential application of zigzag carbon nanotubes in Mg-ion batteries. Struct Chem 31:1073–1078. https://doi.org/10.1007/s11224-019-01485-9
127. Er D, Detsi E, Kumar H, Shenoy VB (2016) Defective graphene and graphene allotropes as high-capacity anode materials for Mg ion batteries. ACS Energy Lett 1:638–645. https://doi.org/10.1021/acsenergylett.6b00308
128. Yu Y, Guo Z, Peng Q, Zhou J, Sun Z (2019) Novel two-dimensional molybdenum carbides as high capacity anodes for lithium/sodium-ion batteries. J Mater Chem A 7:12145–12153. https://doi.org/10.1039/c9ta02650a
129. Guo Z, Zhou J, Sun Z (2017) New two-dimensional transition metal borides for Li ion batteries and electrocatalysis. J Mater Chem A 5:23530–23535. https://doi.org/10.1039/c7ta08665b
130. Meng Y, Wang D, Zhao Y, Lian R, Wei Y, Bian X, Gao Y, Du F, Liu B, Chen G (2017) Ultrathin TiO_2-B nanowires as an anode material for Mg-ion batteries based on a surface Mg storage mechanism. Nanoscale 9:12934–12940. https://doi.org/10.1039/c7nr03493h
131. Levi M, Lancri E, Levi E, Gizbar H, Gofer Y, Aurbach D (2005) The effect of the anionic framework of MoX Chevrel Phase (X=S, Se) on the thermodynamics and the kinetics of the electrochemical insertion of Mg ions. Solid State Ionics 176:1695–1699. https://doi.org/10.1016/j.ssi.2005.04.019
132. Yoo HD, Liang Y, Dong H, Lin J, Wang H, Liu Y, Ma L, Wu T, Li Y, Ru Q, Jing Y, An Q, Zhou W, Guo J, Lu J, Pantelides ST, Qian X, Yao Y (2017) Fast kinetics of magnesium monochloride cations in interlayer-expanded titanium disulfide for magnesium rechargeable batteries. Nat Commun 8:339. https://doi.org/10.1038/s41467-017-00431-9
133. Yang S, Li D, Zhang T, Tao Z, Chen J (2011) First-principles study of zigzag MoS2 nanoribbon as a promising cathode material for rechargeable Mg batteries. J Phys Chem C 116:1307–1312. https://doi.org/10.1021/jp2097026

134. Liu F, Wang T, Liu X, Fan LZ (2020) Challenges and recent Progress on key materials for rechargeable magnesium batteries. Adv Energy Mater 11:2000787. https://doi.org/10.1002/aenm.202000787
135. Ling C, Banerjee D, Song W, Zhang M, Matsui M (2012) First-principles study of the magnesiation of olivines: redox reaction mechanism, electrochemical and thermodynamic properties. J Mater Chem 22:13517. https://doi.org/10.1039/c2jm31122d
136. Chen X, Bleken FL, Løvvik OM, Vullum-Bruer F (2016) Comparing electrochemical performance of transition metal silicate cathodes and chevrel phase Mo6S8 in the analogous rechargeable Mg-ion battery system. J Power Sources 321:76–86. https://doi.org/10.1016/j.jpowsour.2016.04.094
137. Zhang R, Ling C (2016) Unveil the chemistry of olivine $FePO_4$ as magnesium battery cathode. ACS Appl Mater Interfaces 8:18018–18026. https://doi.org/10.1021/acsami.6b03297
138. Tran NA, Do Van Thanh N, Le MLP (2021) Organic positive materials for magnesium batteries: a review. Chemistry 27:9198–9217. https://doi.org/10.1002/chem.202100223
139. Vizintin A, Bitenc J, Kopac Lautar A, Grdadolnik J, Randon Vitanova A, Pirnat K (2020) Redox mechanisms in Li and Mg batteries containing poly(phenanthrene quinone)/graphene cathodes using operando ATR-IR spectroscopy. ChemSusChem 13:2328–2336. https://doi.org/10.1002/cssc.202000054
140. Fan X, Wang F, Ji X, Wang R, Gao T, Hou S, Chen J, Deng T, Li X, Chen L, Luo C, Wang L, Wang C (2018) A universal organic cathode for ultrafast lithium and multivalent metal batteries. Angew Chem 130:7264–7268. https://doi.org/10.1002/ange.201803703
141. Bančič T, Bitenc J, Pirnat K, Kopač Lautar A, Grdadolnik J, Randon Vitanova A, Dominko R (2018) Electrochemical performance and redox mechanism of naphthalene-hydrazine diimide polymer as a cathode in magnesium battery. J Power Sources 395:25–30. https://doi.org/10.1016/j.jpowsour.2018.05.051
142. Bitenc J, Pavcnik T, Kosir U, Pirnat K (2020) Quinone based materials as renewable high energy density cathode materials for rechargeable magnesium batteries. Materials 13. https://doi.org/10.3390/ma13030506
143. Mohtadi R, Mizuno F (2014) Magnesium batteries: current state of the art, issues and future perspectives. Beilstein J Nanotechnol 5:1291–1311. https://doi.org/10.3762/bjnano.5.143
144. Novák P, Shklover V, Nesper R (1994) Magnesium insertion in vanadium oxides: a structural study. Z Phys Chem 185:51–68. https://doi.org/10.1524/zpch.1994.185.Part_1.051
145. Novák P, Desilvestro J (2019) Electrochemical insertion of magnesium in metal oxides and Sulfides from aprotic electrolytes. J Electrochem Soc 140:140–144. https://doi.org/10.1149/1.2056075
146. Ji X, Chen J, Wang F, Sun W, Ruan Y, Miao L, Jiang J, Wang C (2018) Water-activated $VOPO_4$ for magnesium ion batteries. Nano Lett 18:6441–6448. https://doi.org/10.1021/acs.nanolett.8b02854
147. Song J, Noked M, Gillette E, Duay J, Rubloff G, Lee SB (2015) Activation of a MnO_2 cathode by water-stimulated Mg^{2+} insertion for a magnesium ion battery. Phys Chem Chem Phys 17:5256–5264. https://doi.org/10.1039/c4cp05591h
148. Ponrouch A, Frontera C, Barde F, Palacin MR (2016) Towards a calcium-based rechargeable battery. Nat Mater 15:169–172. https://doi.org/10.1038/nmat4462
149. Stievano L, de Meatza I, Bitenc J, Cavallo C, Brutti S, Navarra MA (2021) Emerging calcium batteries. J Power Sources 482:228875. https://doi.org/10.1016/j.jpowsour.2020.228875
150. Hosein ID (2021) The promise of calcium batteries: open perspectives and fair comparisons. ACS Energy Lett 6:1560–1565. https://doi.org/10.1021/acsenergylett.1c00593
151. Monti D, Ponrouch A, Araujo RB, Barde F, Johansson P, Palacin MR (2019) Multivalent batteries-prospects for high energy density: Ca batteries. Front Chem 7:79. https://doi.org/10.3389/fchem.2019.00079
152. Arroyo-de Dompablo ME, Ponrouch A, Johansson P, Palacin MR (2020) Achievements, challenges, and prospects of calcium batteries. Chem Rev 120:6331–6357. https://doi.org/10.1021/acs.chemrev.9b00339

153. Ponrouch A, Bitenc J, Dominko R, Lindahl N, Johansson P, Palacin MR (2019) Multivalent rechargeable batteries. Energy Storage Mater 20:253–262. https://doi.org/10.1016/j.ensm.2019.04.012
154. Shannon RD (1976) Revised effective ionic radii and systematic studies of interatomic distances in halides and chalcogenides. Acta Crystallogr A 32:751–767. https://doi.org/10.1107/s0567739476001551
155. Shannon RD, Prewitt CT (1969) Effective ionic radii in oxides and fluorides. Acta Crystallogr Sect B: Struct Sci Cryst Eng Mater 25:925–946. https://doi.org/10.1107/s0567740869003220
156. Hans Wedepohl K (1995) The composition of the continental crust. Geochim Cosmochim Acta 59:1217–1232. https://doi.org/10.1016/0016-7037(95)00038-2
157. Jacks DS, Stuermer M (2020) What drives commodity price booms and busts? Energy Econ 85:104035. https://doi.org/10.1016/j.eneco.2018.05.023
158. Atoji M (1971) Neutron structure analysis of cubic CaC2and KCN. J Chem Phys 54:3514–3516. https://doi.org/10.1063/1.1675375
159. Ozawa K (ed) (2009) Lithium ion rechargeable batteries. Wiley-VCH. https://doi.org/10.1002/9783527629022
160. Wang D, Gao X, Chen Y, Jin L, Kuss C, Bruce PG (2018) Plating and stripping calcium in an organic electrolyte. Nat Mater 17:16–20. https://doi.org/10.1038/nmat5036
161. Shyamsunder A, Blanc LE, Assoud A, Nazar LF (2019) Reversible calcium plating and stripping at room temperature using a borate salt. ACS Energy Lett 4:2271–2276. https://doi.org/10.1021/acsenergylett.9b01550
162. Nielson KV, Luo J, Liu TL (2020) Optimizing calcium electrolytes by solvent manipulation for calcium batteries. Batter Supercaps 3:766–772. https://doi.org/10.1002/batt.202000005
163. Tchitchekova DS, Monti D, Johansson P, Bardé F, Randon-Vitanova A, Palacín MR, Ponrouch A (2017) On the reliability of half-cell tests for monovalent (Li^+, Na^+) and divalent (Mg2+, Ca2+) cation based batteries. J Electrochem Soc 164:A1384–A1392. https://doi.org/10.1149/2.0411707jes
164. Dugas R, Forero-Saboya JD, Ponrouch A (2019) Methods and protocols for reliable electrochemical testing in post-Li batteries (Na, K, Mg, and Ca). Chem Mater 31:8613–8628. https://doi.org/10.1021/acs.chemmater.9b02776
165. Xu ZL, Park J, Wang J, Moon H, Yoon G, Lim J, Ko YJ, Cho SP, Lee SY, Kang K (2021) A new high-voltage calcium intercalation host for ultra-stable and high-power calcium rechargeable batteries. Nat Commun 12:3369. https://doi.org/10.1038/s41467-021-23703-x
166. Deng X, Li L, Zhang G, Zhao X, Hao J, Han C, Li B (2022) Anode chemistry in calcium ion batteries: a review. Energy Storage Mater 53:467–481. https://doi.org/10.1016/j.ensm.2022.09.033
167. Lv T, Suo L (2021) Water-in-salt widens the electrochemical stability window: thermodynamic and kinetic factors. Curr Opin Electrochem 29:100818. https://doi.org/10.1016/j.coelec.2021.100818
168. Zhang J, Cao Z, Zhou L, Park G-T, Cavallo L, Wang L, Alshareef HN, Sun Y-K, Ming J (2020) Model-based Design of Stable Electrolytes for potassium ion batteries. ACS Energy Lett 5:3124–3131. https://doi.org/10.1021/acsenergylett.0c01634
169. Han C, Li H, Li Y, Zhu J, Zhi C (2021) Proton-assisted calcium-ion storage in aromatic organic molecular crystal with coplanar stacked structure. Nat Commun 12:2400. https://doi.org/10.1038/s41467-021-22698-9
170. Xu X, Duan M, Yue Y, Li Q, Zhang X, Wu L, Wu P, Song B, Mai L (2019) Bilayered Mg0.25V2O5·H2O as a stable cathode for rechargeable Ca-Ion batteries. ACS Energy Lett 4:1328–1335. https://doi.org/10.1021/acsenergylett.9b00830
171. Li Z, Fuhr O, Fichtner M, Zhao-Karger Z (2019) Towards stable and efficient electrolytes for room-temperature rechargeable calcium batteries. Energy Environ Sci 12:3496–3501. https://doi.org/10.1039/c9ee01699f

172. Song H, Li Y, Tian F, Wang C (2022) Electrolyte optimization and interphase regulation for significantly enhanced storage capability in ca-metal batteries. Adv Funct Mater 32:2200004. https://doi.org/10.1002/adfm.202200004
173. Palacin MR (2009) Recent advances in rechargeable battery materials: a chemist's perspective. Chem Soc Rev 38:2565–2575. https://doi.org/10.1039/b820555h